CAPITAL UNIVERSITY OF SCIENCE AND TECHNOLOGY, ISLAMABAD


# pH Responsive Polymeric Blend for Enhanced Solubility, Controlled Release and Therapeutic Optimization of Rosuvastatin

by

Asmaa Jabeen

A thesis submitted in partial fulfillment for the degree of Master of Science

in the

Faculty of Pharmacy
Department of Pharmaceutics

2025

*To my beloved parents, whose heartfelt prayers have been my strength throughout this journey.*

*To my loving husband, for his constant support, patience, and unwavering belief in me.*

*And to my dearest children, your love and laughter have been my greatest motivation.*

# CERTIFICATE OF APPROVAL

## pH Responsive Polymeric Blend for Enhanced Solubility, Controlled Release and Therapeutic Optimization of Rosuvastatin

by

Asmaa Jabeen

(MPH233009)

### THESIS EXAMINING COMMITTEE

| S. No. | Examiner | Name | Organization |
|---|---|---|---|
| (a) | External Examiner | Dr. Masood-ur-Rehman | RIU, Islamabad |
| (b) | Internal Examiner | Dr. Reem | CUST, Islamabad |
| (c) | Supervisor | Dr. Nadia Shamshad Malik | CUST, Islamabad |

Dr. Nadia Shamshad Malik
Thesis Supervisor
September, 2025

Dr. Nadia Shamshad Malik
Head
Dept. of Pharmaceutics
September, 2025

Dr. Muzaffar Abbas
Dean
Faculty of Pharmacy
September, 2025

# *Author's Declaration*

I, **Asmaa Jabeen** hereby state that my MPhill thesis titled "**pH Responsive Polymeric Blend for Enhanced Solubility, Controlled Release and Therapeutic Optimization of Rosuvastatin**" is my own work and has not been submitted previously by me for taking any degree from Capital University of Science and Technology, Islamabad or anywhere else in the country/abroad.

At any time if my statement is found to be incorrect even after my graduation, the University has the right to withdraw my MPhill Degree.

**(Asmaa Jabeen)**

Registration No: MPH233009

# *Plagiarism Undertaking*

I solemnly declare that research work presented in this thesis titled "**pH Responsive Polymeric Blend for Enhanced Solubility, Controlled Release and Therapeutic Optimization of Rosuvastatin**" is solely my research work with no significant contribution from any other person. Small contribution/help wherever taken has been duly acknowledged and that complete thesis has been written by me.

I understand the zero tolerance policy of the HEC and Capital University of Science and Technology towards plagiarism. Therefore, I as an author of the above titled thesis declare that no portion of my thesis has been plagiarized and any material used as reference is properly referred/cited.

I undertake that if I am found guilty of any formal plagiarism in the above titled thesis even after award of MPhill Degree, the University reserves the right to withdraw/revoke my MPhill degree and that HEC and the University have the right to publish my name on the HEC/University website on which names of students are placed who submitted plagiarized work.

**(Asmaa Jabeen)**

Registration No: MPH233009

# *Acknowledgement*

All gratitude is directed towards the Almighty Allah, who is the epitome of generosity and empathy, and His Holy Prophet Mohammad (Peace be upon Him), the most exemplary and illustrious individual ever to grace the Earth. He continues to be a guiding light and a source of wisdom for all of humanity. It is through his blessings that I have found the strength and skill to accomplish this objective.

I express my heartfelt gratitude to my esteemed research supervisor, Dr. Nadia Shamshad, for her invaluable guidance, continuous support, and expert insight throughout this research journey. Her encouragement, constructive feedback, and academic mentorship have been instrumental in shaping this thesis and my growth as a researcher. I would like to express my deepest gratitude to Dr. Natasha Gohar for her invaluable guidance, insightful suggestions, and continuous encouragement throughout the course of my thesis work. I am truly thankful for the time, effort, and expertise she dedicated, which played a vital role in the successful completion of this study.

I am deeply thankful to my beloved parents for their unconditional love, endless prayers, and unwavering support. Your sacrifices and encouragement have always been the foundation of my strength and determination.

To my loving husband, thank you for your patience, understanding, and constant motivation. Your belief in me, even during the most trying times, has been a source of strength and comfort throughout this journey. To my precious children, your love, smiles, and innocent encouragement have been a light in every challenging moment. You have inspired me to keep going and reminded me daily of the purpose behind my hard work. This thesis is not just a milestone in my academic career, but a reflection of the support, love, and belief I have received from those closest to my heart. Thank you all for being part of this journey.

**(Asmaa Jabeen)**

# *Abstract*

This study produced a pH-responsive polymeric hydrogel system to improve rosuvastatin solubility and controlled release. Eleven formulations (F1–F11) were synthesized via free radical polymerization with a combination of chitosan, xanthan gum, CMC Na, acrylic acid, and MBA. Swelling studies conducted under simulated GI conditions (pH 1.2, 7.4) exhibited pH-dependent behavior with swelling in the hydrogels significantly greater ($p < 0.05$) at pH 7.4 indicating specific release in the intestine. Entrapment efficiency of the hydrogels ranged from 68.45% to 94.21% with F10 showing optimum sustained release due to the ratio of polymers and crosslinking density. All the in vitro release studies conducted at pH 7.4 showed greater than 90% release for the optimized formulations. For the in vitro release studies of the optimized formulations the release profiles followed Higuchi ($R^2 > 0.97$) and Korsmeyer–Peppas kinetics which demonstrated release controlled by diffusion. In addition, the Weibull parameters ($\alpha, \beta$) confirmed controlled release profiles for F7, F9, and F10 hydrogels when compared with the pH 1.2 and pH 7.4 studies. FTIR studies confirmed the drug and polymer were compatible and DSC and SEM analysis demonstrated thermal stability and porous morphology of the polymeric hydrogels. Acute toxicity studies conducted in mice demonstrated no significant hematological ($p > 0.05$) or histopathological abnormalities ($p > 0.05$), thus indicating biocompatibility. This hydrogel system demonstrated a significant improvement on solubility of rosuvastatin and pH-controlled release after ingestion which indicates potential as a non-toxic oral delivery platform.

# Contents

# List of Figures

# List of Tables

# Abbreviations and Symbols

| | |
|---|---|
| **AMPS** | 2-Acrylamido-2-Methylpropane Sulfonic Acid |
| **APS** | Ammonium Persulfate |
| **AgNPs** | Silver Nanoparticles |
| **a.u.** | Arbitrary Units (intensity in PXRD) |
| **BCS** | Biopharmaceutical Classification System |
| **CMC-Na / CMC Sodium** | Carboxymethyl Cellulose Sodium |
| **CVD(s)** | Cardiovascular Disease(s) |
| **DSC** | Differential Scanning Calorimetry |
| **EE%** | Entrapment Efficiency Percentage |
| **FTIR** | Fourier Transform Infrared Spectroscopy |
| **HPMC** | Hydroxypropyl Methylcellulose |
| **IPN** | Interpenetrating Polymer Network |
| **LCST** | Lower Critical Solution Temperature |
| **MBA** | N,N'-Methylene Bisacrylamide |
| **NLC** | Nanostructured Lipid Carrier |
| **OH** | Hydroxyl group |
| **PAA** | Poly(Acrylic Acid) |
| **PCL** | Polycaprolactone |
| **PEG** | Polyethylene Glycol |
| **pH** | Potential of Hydrogen |
| **PLA** | Polylactic Acid |
| **PXRD** | Powder X-ray Diffraction |
| **RST** | Rosuvastatin Calcium |
| **SEM** | Scanning Electron Microscopy |

| | |
|---|---|
| **SNEDDS** | Self-Nanoemulsifying Drug Delivery System |
| **TGA** | Thermogravimetric Analysis |
| **TPGS** | D-$\alpha$-Tocopherol Polyethylene Glycol Succinate |
| **XG** | Xanthan Gum |
| **ZP** | Zeta Potential |

# Symbols

| | |
|---|---|
| $N_aOH$ | Sodium Hydroxide |
| $NH_2/NH_3$ | Amino group (neutral / protonated) |
| $\beta$CD /$\beta$-CD | Beta-Cyclodextrin |
| $CH_3/CH_2$ | Methyl / Methylene group |
| °C | Degrees Celsius |
| $2\theta$ | Angle in X-ray diffraction analysis |
| $H_2O$ | Water |
| $COO$ | Carboxylate anion |
| $C = O$ | Carbonyl group |

# Chapter 1

# Introduction

## 1.1 Background

Cardiovascular diseases (CVDs) are the leading cause of death in the world, and CVDs contribute to almost 32% of all deaths globally and result in an estimated 17.9 million deaths worldwide each year, as per the World Health Organization(WHO) [1]. CVDs have emerged as a major challenge in Asia, especially because of urbanization, lifestyle changes, and increasing incidences of diabetes and hypertension. In fact, Asia presently accounts for nearly 60% of all cases of cardiovascular disease in the globe which is the sign of the critical need for the creation of more effective therapies and preventive medications, particularly on this continent [2]. Some of the most effective medications used in the prevention and treatment of cardiovascular disease include rosuvastatin calcium (RST), member of class of the HMG-CoA reductase inhibitors, which are also known as statins.

Rosuvastatin inhibits the synthesis of cholesterol in the liver, reducing cholesterol concentration by a significant margin, and plaque formation in clogged vessels. This reduces the fatal cardiovascular diseases risks like heart attacks and strokes [3]. Along with its cardiovascular action, RST is also used in treatment of familial hyperlipidemia, dyslipidemia, hypertriglyceridemia, atherosclerosis, osteoporosis, benign prostatic hyperplasia, and Alzheimer's disease, hence it a generic drug in clinical practice [4]. Rosuvastatin calcium is a white, slightly water-soluble solid

($7.8mg/mL$ at $37^oC$) with a pKa of 4.6, soluble in organic solvent. Solubility is approximately 1mg/mL in ethanol [5]. Organic solvent-free aqueous solution can be formulated by direct mixing of Rosuvastatin powder in aqueous buffer. RST solubility in phosphate buffer, pH 7.2 is 5mg/mL [6].

The Biopharmaceutics Classification System (BCS) Classified rosuvastatin as class II drug [7], characterized by low solubility and high permeability [8] which makes its oral administration challenging.

Along with its pharmacological significance, RST is faced with the significant limitation due to low aqueous solubility, it absorption is the rate-limiting step in dissolution, limiting oral bioavailability to about 20% [9]. Upon oral administration, the drug is primarily absorbed in the duodenum, an area of basic pH ranging from 6 to 7.5, which is optimal for lipophilic drugs like RST.

Low bioavailability limits the drug's effectiveness, making it a suitable candidate for solubility enhancement strategies such as solid dispersions or hydrogel-based delivery systems [10].

Despite rosuvastatin wide therapeutic applicability, the clinical utility of rosuvastatin is significantly hindered by its physicochemical limitations, particularly poor aqueous solubility. Different mechanisms are used to enhance solubility and bioavailability mainly encompassing hydrogels in drug delivery [11] [12].

## 1.2 Aims and Objectives

### 1.2.1 Aims

To develop chemically crosslinked pH-responsive hydrogel-based drug delivery system with optimized drug incorporation, by utilization of natural and synthetic polymers combination, to improve its solubility, extend its release, and enhance oral bioavailability.

### 1.2.2 Objectives

a) To design and optimize pH-responsive hydrogels for the sustain sustained oral release of rosuvastatin achieve by use of blend of natural polymers—chitosan, carboxymethyl cellulose (CMC), and xanthan gum (XG)—and synthetic components such as acrylic acid (AA) and crosslinkers to form a stable hydrogel network.

b) To overcome the solubility and bioavailability limitations of Rosuvastatin by its incorporation into developed hydrogel matrix, enabling protection in the gastric environment and controlled release in the intestinal tract.

c) To ascertain the pH responsive swelling characters, as well as the in vitro release patterns of the hydrogels under controlled gastrointestinal (GI) circumstances, i.e., acidic and alkaline conditions.

d) To describe the physicochemical, morphological, and thermal characteristics of the hydrogels by a set of analytical strategies, such as Fourier-transform infrared spectroscopy (FTIR), scanning electron microscopy (SEM), differential scanning calorimetry (DSC), thermogravimetric analysis (TGA), and the X-ray diffraction (XRD).

e) To evaluate the biocompatibility and safety of included rosuvastatin hydrogels through acute oral toxicity testing and histopathological assessment in animal models and make sure suitability of oral drug delivery.

## 1.3 Hydrogels

Hydrogels are cross-linked three-dimensional networks with the ability to retain an enormous quantity of water without dissolving the polymer, hence making them ideal for drug delivery[13]. Such systems are capable of being designed to release their payload in response to environmental stimuli such as pH, temperature, or ionic strength [14]. Such pH sensitivity of the hydrogels has also particularly found

utility in the controlled release of drugs such as RST, requiring a particular pH environment to dissolve completely [15].

## 1.4 Stimuli-Responsive Hydrogels

Also named as "smart hydrogels" are advanced polymeric systems capable of undergoing physical or chemical changes in response to specific environmental stimuli. These are a group of polymeric materials that have the capability to exhibit reversible, and intrinsic changes in physical or chemical properties when they are exposed to specific external environmental stimuli. Stimuli-responsive hydrogels are particularly significant in biomedical applications such as drug delivery, tissue engineering, biosensors, and wound healing.

These are highly hydrophilic means capable of absorbing large amounts of water or biological fluids, having stimulus sensitivity so respond to specific stimuli with a change in swelling, solubility, permeability, or structure. These hydrogels are often composed of biocompatible polymers and can be engineered to respond within desired physiological ranges [16].

These stimuli responsive hydrogel can be Temperature-responsive hydrogels, which undergo phase transitions near a critical temperature (e.g., LCST—Lower Critical Solution Temperature). Poly(N-isopropylacrylamide) (PNIPAM) is a widely used thermoresponsive polymer [17]. Enzyme-responsive hydrogels, these hydrogels degrade or change in the presence of specific enzymes which is useful in targeting diseased tissues (e.g., cancer or inflammation) where certain enzymes are overexpressed [18].

Electric/Magnetic Field-responsive hydrogels, These types of hydrogels change conformation or release contents under electromagnetic influence, applied for controlled, externally triggered drug release [19]. Light-responsive hydrogels, these hydrogels are incorporated with light-sensitive moieties that enable spatial and temporal control over behavior. These are utilized in site-specific therapies [20].

pH-responsive hydrogel, specific polymeric combination is established which released entrapped drug at specific pH.

## 1.5 pH-Responsive Hydrogels

Hydrogels can be designed as pH-responsive which contain acidic or basic functional groups that ionize at specific pH levels. Swelling or deswelling depends on the ionization state. These are commonly used in gastrointestinal drug delivery, where pH varies between stomach and intestines. In pH-responsive mechanisms, pH-sensitive polymers are designed to swell and deswell upon specific pH change [21].

Different types of methods utilized for hydrogel preparation such as solvent casting, freeze-drying, and in situ gelation to prepare pH-sensitive hydrogel systems. These methods enable the sustained release of rosuvastatin, enhancing its solubility and bioavailability. The crosslinking density, polymer concentration, and conditions of preparation can all be tailored to obtain the specific drug delivery profile [22].

Therapeutic benefits of pH-responsive polymeric blends related are, improved solubility and absorption, the major therapeutic advantage of employing pH-responsive hydrogels is their capability to considerably enhance the solubility of poorly soluble drugs such as rosuvastatin. Through improved solubility in the stomach and targeted release in the intestines, these hydrogels improve the absorption of the drug and thus its bioavailability [23]. The 2nd most important therapeutic advantage is sustained and controlled release since these hydrogels also support sustained release profiles, such that rosuvastatin is released over an extended duration. This can result in more favorable therapeutic effects by sustaining plasma drug levels in the range of the therapeutic window for longer durations, minimizing dosing frequency. Thus, by increasing bioavailability and decreasing variability in drug release, pH-sensitive polymeric hydrogels can enhance the therapeutic index of rosuvastatin. This makes the drug stronger and reduces side effects, leading to improved patient compliance and therapeutic efficacy [24]. Therefore, it can be inferred that pH-responsive polymeric blend hydrogels have a

tremendous potential in increasing the solubility, bioavailability, and therapeutic index of RST [25]. The potential to customize these systems to deliver rosuvastatin in targeted areas of the gastrointestinal tract means that the drug is absorbed more effectively so better clinical efficacy can be achieved. Ongoing research and development of the hydrogel systems will continue to refine their performance and make them a valuable tool for drug delivery and patient care [26].

pH-sensitive polymeric blend for hydrogels is highly beneficial in enhancing the bioavailability of drugs. The hydrogels may control their enzymatic degradation or morphology based on the change in pH, and this is highly beneficial in drug delivery formulations intended for the gastrointestinal tract [27]. The present research is a result of the most current studies as far as the development of pH-sensitive hydrogels and the role these play in enhancing the therapeutical efficacy of rosuvastatin.

Formulation strategies for this involves polymeric blend selection, choosing a suitable polymer blend plays an important role in formulating an efficient pH-responsive hydrogel system for rosuvastatin delivery. It has been investigated in recent studies to use blends of natural and synthetic polymers for optimum performance [28].

# Chapter 2

# Literature Review

## 2.1 Natural Polymers

Natural polymers are biological macromolecules produced by living organisms, consisting of repeated structural units that are derived from biological monomers. The biopolymers present a wide variety of physicochemical properties and biological functions, rendering them extremely useful in pharmaceutical, biomedical, and industrial contexts. Examples include polysaccharides (e.g., cellulose, chitosan, alginate, xanthan gum), proteins (e.g., gelatin, collagen, silk fibroin), and nucleic acids [29].

Owing to their intrinsic biocompatibility, biodegradability, non-toxic nature, and renewable source, natural polymers have been developed as effective functional materials in drug delivery matrices, tissue engineering scaffolds, and wound healing matrices. Their physicochemical properties—gel-forming potential, mucoadhesiveness, and pH-responsiveness can be utilized for the development of controlled and targeted drug delivery systems [30].

Additionally, the availability of reactive functional groups (e.g., hydroxyl, carboxyl, amino) allows them to be chemically modified, thus allowing control over mechanical strength, degradation rate, and drug release kinetics. Nonetheless,

molecular weight variation, the possibility of microbial contamination, and limited mechanical properties in their native state can limit their use as standalone entities. Thus, natural polymers tend to be blended with synthetic polymers or crosslinked to increase their structural rigidity and performance [31].

## 2.2 Synthetic Polymers

Synthetic polymers are artificial macromolecules created by polymerization reactions using synthetic monomers. Synthetic polymers are widely used in different industries because they have bespoken physicochemical properties, structural flexibility, and predictable behavior. In biomedical and pharmaceutical applications, synthetic polymers are vital materials for the construction of controlled-release drug systems, implantable devices, and tissue engineering scaffolds [32].Typical families of synthetic polymers are polyesters (e.g., polylactic acid [PLA], polyglycolic acid [PGA], polycaprolactone [PCL]), polyamides, polyurethanes, polyacrylates (e.g., poly (acrylic acid) [PAA]), and polyethylene glycols (PEG) [33]. Their properties can be tailored to encompass a vast array of thermal, mechanical, and degradation features by varying molecular weight, level of crosslinking, crystallinity, and copolymer composition. One of the major benefits of synthetic polymers is their functional and structural tunability, whereby properties like solubility, degradation rate, mechanical strength, hydrophilicity, and drug release patterns can be effectively controlled. For example, poly (acrylic acid) is employed in extensive pH-sensitive drug delivery because it contains ionizable carboxylic acids that swell in basic conditions [34].

Synthetic polymers can be synthesized into different shapes such as nanoparticles, microspheres, films, and hydrogels. They are used in pharmaceutical applications as excipients, drug carriers, and matrix-forming agents. They are suitable for advanced therapeutic use due to their reproducibility, uniform quality, and the fact that they can be loaded with stimuli-responsive functions (e.g., temperature, pH, redox) [35].

Nonetheless, some drawbacks may limit their sole biomedical application. These include poor biocompatibility, non-biodegradability, and possible toxicity of degradation products. To overcome such limitations, synthetic polymers are often blended with natural polymers or chemically modified to increase biocompatibility and bio functionality [36].

## 2.3 Rational Design of Hybrid Natural/Synthetic Polymer Systems

The combination of natural and synthetic polymers into hybrid polymeric system is a new strategy to take benefits of the complementary properties of both materials. While natural polymers have inherent biocompatibility, biodegradability, and biological functionality, they tend to be plagued by drawbacks such as poor mechanical strength, high batch-to-batch variability, and limited chemical tunability. Synthetic polymers, on the other hand, are characterized by mechanical robustness, processability, and structural control but lack bioactivity and sometimes raise issues of biocompatibility [37] [38].

The blending of these two categories of polymers facilitates the development of smart biomaterials that avoid single defects while performing better functionally. The systems formed by composite have better mechanical strength, degradative kinetics control, greater drug loading capability, and modifiable physicochemical characteristics, highly applicable for biomedical and pharmaceutical devices [39].

## 2.4 Functional Synergy of Hybrid Polymer Composites

Collaborative functionality is exhibited when polymers are blended into composite includes, Improved Mechanical Strength, synthetic polymers support the

structural network of natural polymers, providing stability in physiological conditions. Controlled Degradation and Swelling, synthetic materials enable control of the swelling ratio and degradation rate to suit application requirements, programmable and environmental-stimulus-sensitive drug release systems. Increased Potential for Functionalization, synthetic polymers offer versatile sites for chemical modification that favor attachment of targeting ligands, imaging probes, or crosslinkers [40].

## 2.5 Significance of pH-Responsive Hydrogels

In pH-responsive hydrogel systems, incorporation of synthetic and biologic polymers combination has shown great promising synergistic functions. These hydrogels are designed to have reversible volume transitions with pH change, greatly advantageous for site-specific drug delivery especially in applications such as the gastrointestinal tract or tumor microenvironment [41].

Natural polymers such as chitosan, xanthan gum contain ionizable functional groups (e.g., amino or carboxyl) that exhibit pH-dependent swelling. By themselves, however, these materials may not be stable and responsive in structure in the long term. When mixed with synthetic polymers such as carboxymethyl cellulose (CMC) (Semi synthetic), poly (acrylic acid) (PAA) or poly (vinyl alcohol) (PVA), the resulting hydrogels exhibit increased crosslinking density, mechanical strength, and pH-sensitivity [42]

The synergistic coupling of protonatable or deprotonatable groups of natural as well as synthetic polymers allows for highly regulated swelling kinetics and drug release patterns. Low pH may maintain the network collapsed through protonation (e.g., chitosan-based platforms), hindering drug release. Ionization of carboxyl moieties (e.g., of PAA or CMC) at higher pH, leading to electrostatic repulsion and swelling of the polymer chains, causes fast drug diffusion [43].

Hybridization of synthetic and natural polymers provides a very versatile platform for the development of intelligent, pH-sensitive hydrogel systems. The composites

leverage the natural polymers' biocompatibility and the synthetic polymers' modifiable mechanics and thereby gain drug-delivery tunability with maintenance of biocompatibility and stability during physiological conditions [44].

Against this background, this research targets a composite hydrogel system made of xanthan gum, chitosan, and carboxymethyl cellulose sodium (CMC-Na), chosen for their complementary physicochemical and biological attributes towards realizing pH-sensitive, solubility-improving drug delivery [45] [46].

## 2.6 Polymer Used in the Study

To achieve enhanced solubility, pH specific response and controlled release, composite of 3 polymers is designed, which includes

### 2.6.1 Xanthan Gum (XG)

Xanthan gum is a high-molecular-weight extracellular polysaccharide resulting from the fermentation of Xanthomonas campestris with carbohydrate substrates like glucose or sucrose. It consists of a -(1→4)-D-glucose backbone, much like cellulose, with trisaccharide side chains consisting of mannose and glucuronic acid units [47]. Xanthan gum possesses excellent pseudoplastic and viscosity-enhancing properties at very low concentrations and is extremely stable in a broad pH range (3–10), ionic strength, and temperature conditions. Its anionic character, because of the carboxylic groups, allows for electrostatic interaction with cationic drugs or polymers and can be used for interpenetrating polymer network (IPN) formation. As a pH-responsive hydrogel, xanthan gum can act as a bio adhesive and gel-forming polymer that responds to pH changes by swelling. With higher pH, ionization of carboxyl groups causes greater electrostatic repulsion and hydration, thus supports greater swelling and release of the drug [48]. Its biodegradability, biocompatibility, and mucoadhesive characteristics make xanthan gum a suitable choice for gastrointestinal drug delivery systems for site-specific release and enhanced bioavailability [49] [50].

### 2.6.2 Carboxymethyl Cellulose Sodium (CMC Sodium)

Carboxymethyl cellulose sodium (CMC-Na) is an anionic polysaccharide derived from the chemical modification of cellulose, normally from plant fibers like cotton or wood pulp. The hydroxyl groups of cellulose are substituted partially with carboxymethyl groups, introducing negative-charge functional groups that exhibit pH-responsiveness and high aqueous solubility[51]. CMC-Na has excellent film-forming ability, biocompatibility, biodegradability, and non-toxicity. In aqueous medium, it shows extensive swelling and thickening effects with strong dependence on the extent of substitution and pH of the surrounding environment. In pH-sensitive hydrogel systems, the ionization of carboxylic acid groups at elevated pH results in greater electrostatic repulsion between polymer chains, causing extensive swelling and promoting controlled drug release. These characteristics evidenced CMC-Na as a beneficial semi-synthetic polymer for site-specific drug delivery system formulations, particularly for intestinal targeting wherein the pH is neutral to basic. Furthermore, its compatibility with other natural and synthetic polymers allows it to perform well in interpenetrating polymer networks (IPNs), providing mechanical stability and drug release kinetics that can be controlled necessary for oral delivery of poorly water-soluble drugs like rosuvastatin[52].

### 2.6.3 Chitosan

Chitosan is a cationic linear polysaccharide produced by partial deacetylation of chitin, a wide-spread component of the exoskeletons of crabs and shrimp. It is composed of mainly -(1→4)-linked D-glucosamine residues along with minor amounts of N-acetyl-D-glucosamine depending on the degree of deacetylation. Chitosan is insoluble in neutral and basic aqueous media but soluble in acidic media (pH $< 6.5$) as protonation of unesterified amino groups takes place[53]. It's pH-dependent solubility is the main characteristic renders chitosan an appropriate polymer for formulating pH-sensitive hydrogels. due to electrostatic repulsion between the amine groups, Chitosan swells and dissolves at lowers pH permitting drug encapsulation at an initial stage. while under basic or neutral conditions, the polymer becomes

insoluble and forms a gel-like matrix that is meant to control drug diffusion[54]. Chitosan is mucoadhesive, biodegradable, and biocompatible and, therefore, also valuable in biomedical applications. Its cationic character allows for ionic bonding with anionic polymers like CMC-Na and xanthan gum to create interpenetrating polymer networks (IPNs) with improved mechanical strength, swelling control, and extended drug release characteristics. Such properties render chitosan highly compatible with colon-delivery and pH-sensitive delivery systems for enhancing the bioavailability of poorly soluble drugs like rosuvastatin[55].

### 2.6.4 Integrative Effects: XG, CMC-Na, and Chitosan

The synergistic combination of xanthan gum (XG), carboxymethyl cellulose sodium (CMC-Na), and chitosan within hydrogel matrices facilitates a cooperative enhancement of the physicochemical and functional properties critical to pH-responsive drug delivery systems. Each of the polymers possesses characteristics that, when combined, enhance their performances in relation to single use.

Xanthan gum, a polysaccharide that is anionic in nature, has high viscosity and gel-forming properties, offering structural fortification and long-term drug entrapment. CMC-Na, another anionic water-soluble polymer, enhances swelling activity due to its carboxyl groups, which enable increased absorption of water and facilitate controlled drug release, particularly in alkaline environments. Chitosan, a cationic polysaccharide, is bioadhesive and mucoadhesive in character with pH-dependent solubility, which rises with acidic pH values and also promotes polyelectrolyte complexation with anionic polymers.

When mixed together, these polymers exhibit a polyelectrolyte complexation effect, primarily between the cationic amino groups of chitosan and the anionic carboxyl groups of XG and CMC-Na[56]. This interaction enhances and promotes hydrogel network's mechanical strength and controls the drug release pattern by forming a pH-sensitive matrix [57]. At acidic/lower pH, the complex is highly compact which guaranteed the minimal drug release, whereas at intestinal pH (7.2), swelling and loosening of the matrix are greater, facilitating controlled and

sustained release of rosuvastatin[58]. Thus, the composite ternary polymeric system provides a synergistic effect that optimizes both the solubilization as well as encapsulated drug's release kinetics.

The blend of these polymers overcomes the constraint of rosuvastatin bioavailability and solubility, and hence it is a viable solution to increase the treatment of cardiovascular disease [59].

## 2.7 Rosuvastatin Delivery Challenges

Rosuvastatin calcium (RST) is an extensively specified statin used in the treatment of hyperlipidemia and cardiovascular diseases. Despite its therapeutic efficacy, rosuvastatin is classified as a Biopharmaceutical Classification System (BCS) Class II drug, characterized by low solubility and high permeability.

Poor aqueous solubility results in low and variable oral bioavailability (20%), posing a significant hedge to achieving optimal therapeutic effects. Also, its first-pass metabolism and short half- life further necessitate novel delivery systems to enhance its therapeutic effectives [60]. All the literature review is shown as in Table 2.1.

## 2.8 Novelty and Significance of Proposed Work

While several different advanced delivery systems for rosuvastatin (such as nanogels, vesicular carriers, lipid-based formulations, and transdermal patches) have been investigated, these approaches generally address only one specific challenge (e.g., improving solubility using cyclodextrins or avoiding first-pass metabolism via non-oral routes), while a key unmet need remains: the design of an oral pH-sensitive hydrogel system that simultaneously addresses the poor aqueous solubility, degradation in acidic gastric conditions, and variable intestinal absorption of rosuvastatin.

A pH-responsive oral hydrogel formulation based on xanthan gum (XG), carboxymethyl cellulose sodium (CMC-Na) and chitosan is proposed for the following characteristics:

a) A pH-responsive release behavior allowing resistance to acid degradation during gastric passage while swelling in intestinal pH conditions for targeted drug delivery

b) Enhanced structural integrity due to the formation of interpenetrating polymer networks (IPNs), which can lead to sustained and controlled drug delivery

c) Tunable release kinetics derived from the combination of natural polymer biocompatibility with synthetic crosslinkers that gives rise to specific control over drug release profile

The integrated multi-mechanistic strategy is expected to greatly improve the oral bioavailability of rosuvastatin, representing an innovative alternative to existing formulations.

By targeting multiple pharmacokinetic characteristics, to tackle this complex issue, we developed a novel tri-polymer-based oral hydrogel formulation composed of xanthan gum (XG), carboxymethyl cellulose sodium (CMC-Na) and chitosan with the following features:

a) pH-responsive release behavior that allows for resistance to acid degradation during gastric passage while swelling in intestinal pH conditions for targeted drug deliver

b) Enhanced structural integrity provided by the formation of interpenetrating polymer networks (IPNs), which can lead to sustained and controlled drug delivery

c) Tunable release kinetics obtained from the combination of natural polymer biocompatibility

TABLE 2.1: Summary of Recent Studies on RST Using Polymeric and Lipid - Based Drug Delivery Systems (2024 - 2020)

| **Author(s), Year** | **Polymers / Materials Used** | **Formulation** | **Objective** | **Key Outcomes** |
|---|---|---|---|---|
| Soha M. El-Masry et al., 2024 [61] | Oleic acid, Chitosan | Ufasomal Topical Gel | Diabetic wound healing | Chitosan-coated ufasomes exhibited strong wound healing potential; confirmed via histopathology. |
| Tamer M. Shehata et al., 2024 [62] | Virgin Coconut Oil (CCO), Tween 80 | Nanostructured Lipid Carrier (NLC) | Enhance hypolipidemic effect | Significant reduction in lipid profile; synergistic effect of CCO with Rosuvastatin (RST). |
| Sidra Younus et al., 2024 [63] | Soy phosphatidylcholine (SPC), Tween 80 (T80), Sodium cholate (SC), Carbopol 940 | Rosuvastatin calcium-loaded transfersomes (ROS-TFs) | Potential transdermal application | Sustained drug delivery; improved patient compliance and bioavailability. |
| Hina Shoukat et al., 2024 [6] | $\beta$-Cyclodextrin ($\beta$-CD), Poloxamer-407, AMPS | Interpenetrating Polymer Network (IPN) Nanogel | Enhance solubility and oral bioavailability | High biocompatibility, solubilization, and physicochemical stability. |
| Syed F. Badshah et al., 2023 [64] | $\beta$-Cyclodextrin ($\beta$-CD) | Polymeric Nanogel | Solubility enhancement | High swelling, solubilization, and controlled drug release properties. |
| Islam M. Adel et al., 2023 [65] | Dialysis cellulose membrane, Chitosan, Sodium alginate | Rosuvastatin calcium-loaded silica nanoparticles | Jaw bone healing/regeneration | Sustained delivery; effective in healing bone tissue damage. |
| R. González et al., 2022 [7] | Lactose monohydrate, Microcrystalline cellulose, Dibasic calcium phosphate | Amorphous oral tablet (direct compression) | Dissolution enhancement | Adequate stability and bioavailability; rapid drug release. |
| Heba F. Salem et al., 2021 [66] | Lecithin, Poloxamer 407 | Nanocubic Vesicles + AgNPs-Loaded Gel | Enhance skin performance, antimicrobial action | Promising for wound healing and tissue repair. |
| Tarek A. Ahmed et al., 2021 [67] | l-$\alpha$-Soybean phosphatidylcholine, Tween 80, Acetonitrile, Aspartame | Lyophilized orodispersible tablets (transfersome nanoparticles) | Enhance rosuvastatin bioavailability and hypolipidemic activity | Hepatoprotective effects. |

Continued on next page

**Table 2.1 continued from previous page**

| Author(s), Year | Polymers / Materials Used | Formulation | Objective | Key Outcomes |
|---|---|---|---|---|
| Nabila M. Sweed et al., 2020 [68] | Surfactant/co-surfactant mix and oil | Self-Nanoemulsifying Drug Delivery System (SNEDDS) | Improve solubility and anticancer activity | SNEDDS formulation showed enhanced anticancer potential. |
| Ibrahim Elsayed et al., 2020 [69] | Tween 80, Cetyl Alcohol, Clove Oil, Carboxymethyl Cellulose (CMC) | Elastic Nanovesicular Gel | Enhance bioavailability and anticancer efficacy | Improved permeability, entrapment, and controlled release. |
| Khaled M. Hosn et al., 2020 [70] | Lecithin, Tween 80, D-$\alpha$-Tocopherol Polyethylene Glycol Succinate (TPGS) | In Situ Gel (Nanotransferosomes) | Anticancer activity for tongue carcinoma | Boosted bioavailability and induced apoptosis via caspase-3 and P21 tumor. |

# Chapter 3

# Materials and Methods

## 3.1 Materials

Rosuvastatin calcium was supplied in generous donations from Jupiter Pharmaceuticals (Pvt.) Ltd., Islamabad, Pakistan. Chitosan (medium molecular weight; 75% deacetylated), xanthan gum, and sodium carboxymethyl cellulose (CMC Na) were purchased from Sigma-Aldrich, USA. Ammonium persulfate (APS), acrylic acid (AA), and N, N -methylenebisacrylamide (MBA) were purchased from Shouguang Pner Chemical Co., Ltd., China. Potassium dihydrogen phosphate (KH2PO4), disodium hydrogen phosphate (Na2HPO4), and sodium hydroxide (NaOH) were analytical reagents purchased from Merck, Germany, and used for buffer preparation. Acetone and glacial acetic acid were obtained from Sigma-Aldrich, USA. The distilled water used in the experiments was prepared by the Faculty of Pharmacy of Capital University of Science and Technology Islamabad, Pakistan, and given to the researchers. Chemicals and reagents were of analytic quality as was indicated and were used as received, without further purification.

## 3.2 Method

Interpenetrating polymeric network (IPN) hydrogels composed of acrylic acid (AA), xanthan gum, chitosan, and sodium carboxymethyl cellulose (CMC Na) were synthesized via free radical polymerization, employing a systematic approach for uniform network formation [64] as shown as Figure 3.1.

The preparation of Beaker A commenced with dissolving accurately measured amounts of xanthan gum (ranging from 1g to 3g) and CMC Na (also 1g to 3g) in an adequate volume of distilled water. This mixture was continuously agitated on a hot plate and gently warmed to approximately 50 degrees Celsius to facilitate complete polymer dissolution, resulting in a clear and homogeneous solution. After total hydration, the solution was allowed to cool to room temperature while maintaining constant agitation to ensure uniform polymer distribution.

In a separate procedure, Beaker B was prepared by dissolving chitosan (1–3 g) in a 1% (v/v) acetic acid solution under continuous stirring until a clear, homogeneous mixture was achieved. The contents of Beaker A were then gradually added to Beaker B with consistent stirring to produce a homogeneous blended polymeric solution. This resulting mixture was maintained on a magnetic stirrer at 50 °C to promote optimal polymer interaction. Subsequently, a freshly prepared aqueous solution of $N, N$-methylenebisacrylamide (MBA, $0.20.4g$) as the cross-linker and ammonium persulfate (APS,$0.2g$) as the free radical initiator was added dropwise to the polymeric blend while stirring continuously. The addition of these components initiated free radical generation, marking the onset of free radical polymerization and facilitating subsequent polymer cross-linking. Acrylic acid (AA, 6g-10g) was gradually introduced into the reaction mixture at a temperature of 50°C while stirring. This controlled addition of the monomer promoted a more homogeneous polymerization process. Following this, the entire mixture was thoroughly homogenized at 600 rpm in the laboratory to eliminate entrapped air and ensure a uniform distribution of components, thus enhancing the consistency of the cross-linked network throughout the matrix.

The polymer solution was then carefully poured into sterile, dry glass test tubes that acted as molds. These were incubated at 60 °C for 5 hours. This final step concluded the free radical polymerization process, resulting in a robust interpenetrating polymeric network. After the completion of the polymerization, hydrogels were left at room temperature, then removed from their molds, and shaped into disc forms with a diameter of $8.00 \pm 0.05$ mm and a thickness of $2.00 \pm 0.03$ mm. Freeze-drying (-55 °C, 0.01 mbar) was performed on a lyophilizer to remove any excess water, enhance porosity, and stabilize the network for further characterization and drug loading studies. Composition of formulated hydrogels are as shown as Table 3.1.

TABLE 3.1: Concentrations of polymer, monomer, cross-linker, and initiator used in the synthesis of hydrogels

| **Formulation** | **Chitosan (g)** | **Xanthan Gum (g)** | **CMC Sodium (g)** | **Acrylic Acid (g)** | **MBA (g)** | **APS (g)** |
|---|---|---|---|---|---|---|
| F1 | 2.0 | 2.0 | 2.0 | 6.0 | 0.2 | 0.2 |
| F2 | 1.0 | 2.0 | 2.0 | 6.0 | 0.2 | 0.2 |
| F3 | 3.0 | 2.0 | 2.0 | 6.0 | 0.2 | 0.2 |
| F4 | 2.0 | 1.0 | 2.0 | 6.0 | 0.2 | 0.2 |
| F5 | 2.0 | 3.0 | 2.0 | 6.0 | 0.2 | 0.2 |
| F6 | 2.0 | 2.0 | 1.0 | 6.0 | 0.2 | 0.2 |
| F7 | 2.0 | 2.0 | 3.0 | 6.0 | 0.2 | 0.2 |
| F8 | 2.0 | 2.0 | 2.0 | 8.0 | 0.2 | 0.2 |
| F9 | 2.0 | 2.0 | 2.0 | 10.0 | 0.2 | 0.2 |
| F10 | 2.0 | 2.0 | 2.0 | 6.0 | 0.3 | 0.2 |
| F11 | 2.0 | 2.0 | 2.0 | 6.0 | 0.4 | 0.2 |

## 3.3 Drug Loading

Drug loading was performed by immersing hydrogel discs (diameter: 8.00 ± 0.05 mm, thickness: 2.00 ± 0.03 mm, weight: 0.92 ± 0.03 g, n = 3) of predetermined

weight into a 1.0% w/v solution of Rosuvastatin in phosphate buffer at pH 7.4. The discs were subsequently washed three times (for 30 seconds each) with 10 mL of deionized water to remove any adsorbed drug or debris from their surface.

After washing, the surface was blotted dry using Whatman® Grade 1 filter paper. The discs were then dried for 48 hours under vacuum at -55°C and 0.01 mbar within a lyophilizer, ensuring the prevention of moisture retention and structural degradation.

Finally, the dried, drug-loaded discs were stored in vacuum desiccators at 25°C with a relative humidity below 10 percent until further testing could be performed [71].

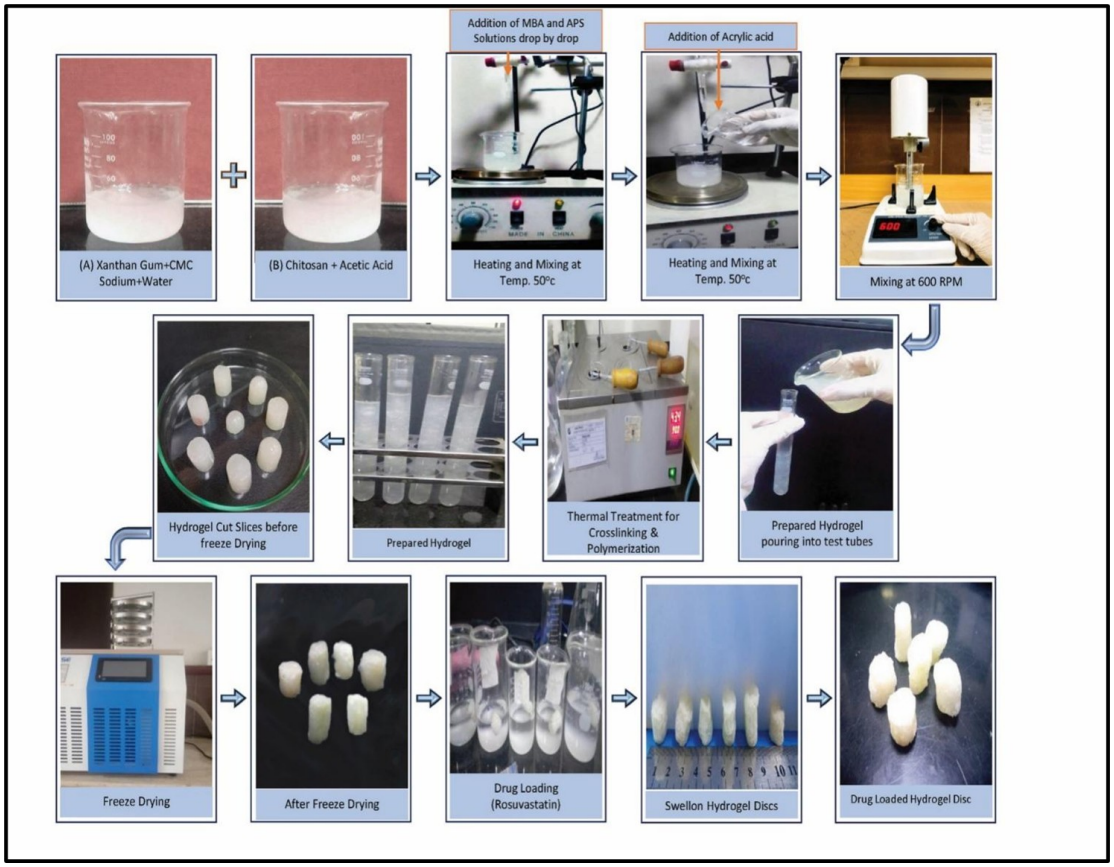


FIGURE 3.1: Schematic outline of the process of hydrogel synthesis

The path followed was to create polymer solutions, (Xanthan Gum + CMC or Chitosan + Acetic Acid), in addition to crosslinking via MBA (N, N'-Methylenebisacry lamide) and APS (Ammonium Persulfate)—acrylic acid was also added at this stage—then polymerizing via thermal methods at 50 degrees Celsius, casting into

molds, freeze-drying to porous up the hydrogels, and ultimately loading drug (Rosuvastatin). The cross-linkable networks of the hydrogel were achieved through intentionally controlled physicochemical cross-linking.

## 3.4 Characterization

### 3.4.1 Physical Appearance and Structural Evaluation of Hydrogels

The developed hydrogel's physical appearance and structural integrity comprehensively characterized using standardized characterization procedures to ensure consistency, reproducibility, and formulation quality. Freshly prepared hydrogels were macroscopically examined for clarity, color, surface uniformity, and absence of visible imperfections such as cracks, air entrapment, or phase separation. To evaluate the internal structural integrity and hydrogels, stability more effectively, samples were freeze dried in a laboratory freeze-dryer (Christ Alpha, Germany). Hydrogel discs were frozen at -80 °C for 24 h before lyophilization to ensure complete solidification. Lyophilization took place for 48 h under a vacuum of 0.01 mbar to remove any residual moisture without disrupting the polymeric network. The freeze-dried hydrogel discs were subsequently analyzed for physical appearance alterations, including texture, porosity, and structural shrinkage. These observations provided information into the interconnected porous matrix's formation, which is critical step for drug loading, swelling characteristics, and controlled release performance. All analyses were repeated in triplicate, and only hydrogels meeting the predetermined physical and structural criteria were selected for further physicochemical, mechanical, and biological investigations[71].

### 3.4.2 Drug Encapsulation Efficiency (EE%)

Standardized experimental protocols were employed to ensure reproducibility across all investigations [72]. Hydrogel discs with uniform dimensions (diameter: 8.00

± 0.05 mm, thickness: 2.00 ± 0.03 mm) were fabricated for all evaluations. The dimensional accuracy of each disc was confirmed using a precision digital caliper. A calibrated analytical balance was utilized to provide a consistent disc mass at $0.95 \pm 0.01$ g (n = 3 individual batches), providing consistency in experimental groups. Discs with these specified requirements were employed for subsequent analyses. To evaluate encapsulation efficiency (EE%) of drug-loaded hydrogels accurately weighing standard hydrogel discs were finely ground using a mortar and pestle. Powdered hydrogel was dispersed in 100 mL phosphate buffer solution (pH 7.4) and was equilibrated for 24 h to allow extraction of the drug. The dispersion was ultrasonicated for 20 minutes to allow release of the drug from the polymeric matrix. Residual polymeric debris was removed via centrifugation at 3000 rpm, and rinsed with fresh phosphate buffer to ensure complete recovery of unbound drug[73]. The clear supernatant was scanned for RST content using a UV-Visible spectrophotometer at a characteristic wavelength ( max) of 243 nm. The encapsulation efficiency was calculated by the following equation 1:

$$\text{EE\%} = \left( \frac{\text{Amount of drug entrapped}}{\text{Total amount of drug initially used}} \right) \times 100 \tag{3.1}$$

### 3.4.3 In Vitro Swelling Studies

Rosuvastatin-loaded hydrogel's swelling behavior was evaluated, to assess their fluid absorption capacity and structural integrity[74]. Pre-weighed, lyophilized hydrogel discs with average ($8.00 \pm 0.05$ mm diameter, $2.00 \pm 0.03$ mm thickness, $0.92 \pm 0.03$ g) were selected for the study. The initial dry weight of each sample (W ) was measured by calibrated analytical balance. The hydrogel discs were immersed in an excess volume of phosphate buffer (pH 7.4) at $37 \pm 0.5$ °C to simulate physiological conditions. To facilitate unrestricted swelling and prevent premature dehydration, the medium volume was kept sufficiently high relative to the sample size. At predetermined time intervals (1 hour, 2 hours, and 24 hours), the samples were carefully removed from the swelling medium, gently blotted with filter paper to remove surface-adhered water and weighed to determine the swollen hydrogel mass (W ). The swelling ratio (q) was calculated using the following equation 2:

$$q = \left( \frac{W_1 - W_0}{W_0} \right) \times 100 \tag{3.2}$$

Where,

$W_1$ = Weight of swollen hydrogel

$W_0$ = Weight of the dry hydrogel

### 3.4.4 In Vitro Drug Release Study and Release Kinetics

The in vitro drug release profile for rosuvastatin-loaded hydrogels was studied with the United States Pharmacopeia (USP) dissolution apparatus II (paddle method) [75]. using simulated gastric fluid pH 1.2 and phosphate buffer pH 7.4 as dissolution media, at a temperature of $37 \pm 0.5\,^{\circ}\mathrm{C}$ and a paddle rotation speed of 90 rpm throughout all the experiments.

Throughout the experiment, the dissolution medium volume was held constant at 900 mL, and the temperature was kept constant at $37 \pm 0.5\,^{\circ}\mathrm{C}$ to simulate physiological conditions.

At predetermined time intervals, 5 mL aliquots were withdrawn from the dissolution vessel and replaced with an equal volume of fresh, preheated dissolution medium to maintain sink conditions and constant volume.

Filtered samples were analyzed, and the release of Rosuvastatin was quantitated using UV–visible spectrophotometer (UV 3000, Germany) at 243 nm ( max). All experiments were performed in triplicate, and the results are presented as mean ± standard deviation. Cumulative drug release data were also fitted to various kinetic models, including zero-order, first-order, Higuchi, and Korsmeyer–Peppas models, to determine the drug release mechanisms from the hydrogel matrix [76].

### 3.4.5 Fourier Transform Infrared Spectroscopy

Fourier Transform Infrared (FTIR) spectroscopy was employed to describe the presence of characteristic functional groups' occurrence and identify any probable interaction between the drug and polymeric materials. Unloaded and RST-loaded hydrogel samples, carboxymethyl cellulose (CMC) sodium, chitosan, xanthan gum, acrylic acid, ammonium persulfate (APS), and N,N -methylenebisacrylamide (MBA), and pure rosuvastatin calcium were characterized through spectral methods. Measurements were made on an attenuated total reflectance FTIR spectrometer (ATR-FTIR; Bruker Tensor 27 series, Ettlingen, Germany). Background spectrum acquisition for atmospheric as well as for instrumental interferences was achieved by using an empty cell prior to sample acquisition. Solid and liquid samples were accurately positioned onto a Pike Miracle ATR cell with a zinc selenide (ZnSe) crystal. For best contact and spectral resolution, the assembly was gradually rotated to achieve a dense and uniform sample layer. Spectral data were recorded between the wavenumber range of 4000 to 650 $cm^{-1}$ .Based on the spectra, the characteristic vibrational bands attributable to functional groups were analyzed for Rosuvastatin (O-H/N-H stretching at ($\sim 3400\ cm^{-1}, C = Ostretchingat(\sim 1650\ cm^{-1})$, aromatic C=C vibrations at $\sim 1600\ cm^{-1}$) and the hydrogel polymer (e.g. carboxylic acid C=O stretching at $\sim 1700\ cm^{-1}$ for poly (acrylic acid) based hydrogels). A comparative spectral analysis was performed to assess possible interactions (e.g. hydrogen bonding or electrostatic forces), which is evidenced by peak shifts, broadening or disappearance of the peaks [77].

### 3.4.6 Powder X-ray Diffraction

Powder X-ray Diffraction (PXRD) was utilized in examining the phase nature and structural properties of individual ingredients and nanogel ingredients. The technique is significant in differentiating amorphous and crystalline states, their implications reaching drug solubility and bioavailability. In the current research, pure Rosuvastatin calcium XRD patterns, Chitosan, Carboxymethyl Cellulose Sodium,

Xanthan Gum, placebo hydrogels, and drug-loaded nanogels were achieved. Samples were harvested by keeping dried hydrogel powders in the sample holder in a manner that it has a flat and even surface to analyze. Diffraction scans were captured from 2  range of 0° to 60° with 5°/min scanning rate. The diffractograms thus obtained were analyzed to establish the physical form (crystalline or amorphous) of each constituent and formulations [78].

### 3.4.7 Thermal Analysis

Thermal tests carried out for evaluating thermal stability and compatibility of Rosuvastatin calcium with chosen polymers and for determining the integrity of the polymer–monomer matrix in developed hydrogel formulations. Differential Scanning Calorimetry (DSC) and Thermogravimetric Analysis (TGA) were done with pure drug, individual polymers, and developed hydrogels. TGA was conducted with sample weights between 0.5 and 5 mg. The experiment was performed in a continuous stream of nitrogen at the same flow rate of 10 mL/min. The samples were heated under a constant heating rate of 20 °C/min from room temperature to 600 °C to evaluate thermal degradation behavior [79]. DSC was conducted in the range of 0–600 °C at a heating rate of 20 °C/min. A purge flow rate of 20 mL/min nitrogen was used to create an inert atmosphere and avoid oxidative decomposition. The obtained thermograms were evaluated to identify thermal transitions such as melting point, glass transition temperature (Tg), and decomposition profiles [80]

### 3.4.8 Scanning Electron Microscopy

The surface morphology and internal microstructure of the rosuvastatin-loaded pH-responsive hydrogel is evaluated by scanning electron microscopy (SEM) including the assessment of structural aspects, porosity, surface topography, and drug distribution. After washing the hydrogel samples with distilled water to remove unreacted material and freeze-dried using a freeze-dryer to remove moisture while maintaining the original architecture, the freeze-dried hydrogels were sliced

into thin cross-sections (2–3 mm thick) using a sharp blade to expose the internal matrix structure. The samples were affixed to aluminum stubs by means of the double-sided conductive carbon tape to ensure sample adhesion and reduce the effect of charging when the electron beam is directed through the sample. SEM analysis was carried out using a high-vacuum field-emission scanning electron microscope set at accelerated voltages from 5–15 kV and a working distance of 8–12 mm. The secondary electron (SE) imaging mode was employed to capture topographic features to allow for comparison at varying magnification. Each sample was analyzed three times way of triplicate samples subjected to the same instrument settings to ensure reproducibility [65].

### 3.4.9 Acute Oral Toxicity Study

An acute oral toxicity study was conducted as per compliance with the OECD Guideline 423 (Acute Toxic Class Method). The standard study protocol was reviewed and approved by the Institutional Research Ethics Committee of the Faculty of Pharmacy, Capital University of Science and Technology (CUST), Islamabad, Pakistan (Approval No. REC/FoP/F2024/05).

The study intended to investigate the safety profile of the optimized Rosuvastatin-loaded hydrogel formulation. A total of ten healthy adult female Balb/c mice (9–10 weeks old, average body weight $21 \pm 2$ g) were obtained from the Animal Facility Center of CUST. Female animals were selected based on their recognized sensitivity to toxicological evaluations. The animals were housed under controlled laboratory conditions, i.e. controlled temperature ($25 \pm 2$ °C), relative humidity ($65 \pm 5\%$), and a 12-hour light/dark cycle. Standard laboratory diet and water were supplied ad libitum. Prior to the experiment the animals were acclimatized in laboratory environment for seven days.

After acclimatization phase, the animals were randomly divided into two groups (n = 5 per group):

a) Group A (Control group): Given 0.9% normal saline at a dose volume of 1 mL/100 g body weight via oral gavage.

b) Group B (Treatment group): Administered with the optimized Rosuvastatin-loaded hydrogel formulation at a dose of 2 g/kg body weight, administered orally via gavage.

To avoid excessive dosing volume and discomfort, the entire dose of 2 g/kg was split into three equal units and administered every 30 minutes. The hydrogel formulation was suspended in normal saline to achieve the desired dosing volume of 1 mL/100 g body weight.

All animals were observed individually following doses, with particular attention paid to the first four hours of post-administration. Follow up daily observations were made for 14 consecutive days to observe potential signs of toxicity. Clinical observations included assessment of general appearance (skin, fur, mucous membranes, and eyes), behavioral patterns (salivation, tremors, sleep abnormalities, diarrhea, coma), and neurological manifestations (postural changes, gait abnormalities, stereotypic movements such as grooming or circling).

Food and water consumption of each animal were measured daily. On day 15, animals were anesthetized via an intraperitoneal injection of ketamine (100 mg/kg) and xylazine (10 mg/kg) then euthanized via cervical dislocation. Blood samples were collected through cardiac puncture into EDTA-coated tubes for hematological investigation. Vital organs (heart, liver, kidneys, spleen and stomach) were removed surgically, rinsed with ice-cold saline, and macroscopically inspected for any visible gross abnormalities or lesions. The organs were weighed by using analytical balance, preserved in 10% neutral-buffered formalin for 48 hours in glass jar and processed for histopathological assessments. Paraffin-embedded tissue sections (5 $\mu$m) stained with hematoxylin and eosin (H&E) and analyzed under a light microscope for evaluation of drug induced microscopic alterations [81].

## 3.5 Statistical Analysis

All experimental data were expressed as mean ± standard deviation (SD). Statistical analyses were performed using SPSS® software. For multiple group comparisons, one-way analysis of variance (ANOVA) followed by appropriate post hoc tests were applied. For pairwise comparisons, Student's t-test was used. A p-value of less than 0.05 was considered statistically significant.

# Chapter 4

# Results and Discussion

## 4.1 Physical Appearance and Structural Evaluation of Hydrogels

To investigate the effect of polymer composition and concentration on physical and structural properties, hydrogel discs were prepared by free radical polymerization and chemical crosslinking using a combination of chitosan, carboxymethyl cellulose sodium (CMC-Na), and xanthan gum.

The newly synthesized hydrogels had a clear to slightly opaque appearance, depending on the ratio of the used polymers (Figure 4.1), indicating good dispersion and solubilization of the hydrogel components.

After drying and storage at room temperature for 24 h, all formulations turned a milky-white color that indicated the formation of polymeric networks and partial dehydration of the hydrogel matrix, as reported previously for polysaccharide-based hydrogels because of structural reorganization during solvent loss. Macroscopic evaluation showed formulation-dependent differences in texture, transparency, stickiness, and uniformity which are summarized in Table 4.1. This is particularly important for hydrogel-based drug delivery systems as the matrix consistency and surface integrity directly influence drug entrapment, swelling, and release behavior [82].

FIGURE 4.1: Freshly prepared chitosan, CMC-Na, and xanthan gum-based hydrogels.

Freshly prepared chitosan, CMC-Na, and xanthan gum-based hydrogels exhibiting clear to slightly opalescent characteristics, which transitioned to a uniform milky white color upon drying and storage, confirming successful network formation

TABLE 4.1: Physicochemical Characterization of Hydrogel Formulations

| **Code** | **Appearance** | **Texture** | **Color** | **Stickiness** | **Uniformity** |
|---|---|---|---|---|---|
| F1 | Transparent | Smooth | Pale yellow | Low | Uniform |
| F2 | Opaque | Gelatinous | Yellowish | Moderate | Uniform |
| F3 | Slightly hazy | Firm | Yellow | Low | Uniform |
| F4 | Clear | Soft | Light yellow | High | Non-uniform |
| F5 | Transparent | Smooth | Yellowish | Low | Uniform |
| F6 | Clear | Elastic | Pale yellow | Low | Uniform |
| F7 | Slightly opaque | Firm | Yellow | Moderate | Uniform |
| F8 | Slightly opaque | Rigid | Dark yellow | High | Non-uniform |
| F9 | Opaque | Rigid | Yellow | Low | Uniform |
| F10 | Hazy | Smooth | Pale yellow | Moderate | Uniform |
| F11 | Clear | Soft | Light yellow | Low | Uniform |

Hydrogel formulations exhibits distinct characterization which are in direct correlation with their compositional variations as shown as Figure 4.2. Balanced polymer concentrations (F1; 2 g each) produced transparent, smooth hydrogels with well-organized polymeric networks, whereas decreased chitosan content (F2; 1 g) led to an opaque, more viscous structure likely due to fewer ionic interactions and impaired gelation.

Alternatively, xanthan gum concentration had a major effect on morphology: lower concentrations (F4; 1 g) gave clear but non-uniform hydrogels because of insufficient entanglement, while increased loading (F5; 3 g) enhanced viscosity and matrix density by increasing chain interactions

The CMC-Na also influenced hydrogel characteristics; lower concentrations (F6: 1 g) gave elastic, flexible discs while higher concentration (F7: 3 g) produced firmer, stiffer hydrogels with more crosslinking and increased hydrogen bonding between polymer chains.

FIGURE 4.2: Visual representation of hydrogel formulation discs showing physical appearance, transparency, color variation, and surface texture

The effect of the crosslinker was also evident from F8 (0.3 g MBA), which produced uneven, too hard structures, and F9 (0.4 g MBA), which generated opaque, dense discs, suggesting excessive crosslinking and low chain mobility.

Changes in acrylic acid concentration showed opposite effects: F10 (8 g AA) was slightly hazy, presumably because of early-stage phase separation, while F11 (10 g AA) unexpectedly became clear again, possibly because of better solvation and extended polymer chains ordering into more organized structures.

While pH and viscosity measurements were not performed in this study, qualitative assessments of surface stickiness and appearance yielded useful information regarding the structural coherence of the hydrogels; increased stickiness in F4 and F8 correlated with decreased crosslinking density or insufficient polymer content, leading to looser, less cohesive networks. Taken together, the physical attributes

clearly demonstrate that compositional variation can have a significant impact on hydrogel formation, morphology, and mechanical properties, which is fundamental to understanding how to optimize hydrogels for oral drug delivery applications in which consistent network integrity and physicochemical performance are critical [83].

## 4.2 Drug Encapsulation Efficiency (%EE)

Each of rosuvastatin-loaded hydrogel formulations (F1–F11) was evaluated %EE to determine the polymeric network's capability in effectively retaining the drug. UV spectrophotometric analysis at 240 nm revealed EE values ranging from 81.23% to 93.43%, confirmed successful drug incorporation across all formulations as shown as Table 4.2.

TABLE 4.2: Entrapment Efficiency (EE) of Rosuvastatin-Loaded Hydrogel Formulations

| **Formulation** | **Entrapment Efficiency (%) ± SEM** |
|---|---|
| F1 | 81.48 ± 1.15 |
| F2 | 79.95 ± 1.40 |
| F3 | 84.32 ± 1.25 |
| F4 | 75.66 ± 1.50 |
| F5 | 93.43 ± 1.35 |
| F6 | 81.02± 1.50 |
| F7 | 86.50 ± 1.30 |
| F8 | 88.10 ± 1.20 |
| F9 | 80.23 ± 1.45 |
| F10 | 82.70 ± 1.25 |
| F11 | 88.14 ± 1.10 |

F4 (75.66 ± 1.50%) exhibited the lowest EE%, which was significantly lower ($p$<0.05) than all other formulations. The decreased xanthan gum (1 g) content

resulted in a reduction in gel network strength and as a result, more sol fraction, that led to drug diffusion/loss while synthesizing or during washing steps. F2 (79.95 ± 1.40%) had a non-significantly higher EE content than F4 ($p$>0.05) but still had a lower EE than F1 and other relevant formulations. Due to the decreased concentration of chitosan (1 g) earlier formulations with higher molar concentrations of chitosan likely had stronger electrostatic interactions between amino groups of chitosan and acidic drug (rosuvastatin), limiting the ability to entrap [84]. The EE of F9 (80.23 ± 1.45%) is demonstrated as moderate, although having statistically non-significant difference ($p > 0.05$) compared to F1 and F6. The higher MBA content (0.4 g) may have caused over-crosslinking and a rigid matrix with reduced porosity is created, [85] which could have decreased drug diffusion into the gel structure and thereby slightly compromised EE. F6 (81.02 ± 1.50%) also had similar EE to F1, with a non-significant difference ($p > 0.05$). The lower EE may have been due to the lower CMC sodium content (1 g) which influenced the hydrogel's swelling capacity; limiting drug solubilization and entrapment during formation. F1 (81.48 ± 1.15%) containing a balanced set of polymer quantities (2g of each polymer), also demonstrated moderate EE as a reference point of comparison. This formulation was able to create a more uniform gel network that was facilitated by the equimolar polymer ratio. This indicated effective drug encapsulation but lower than enhanced effects obtained from ultimately polymer-optimized or cross-linker-optimized systems [86]. F10 (82.70 ± 1.25%) showed significant differences ($p < 0.05$) from F4 and F2 AA systems and showed almost equivalent efficacy in comparison to F1, F6, and F9 EE values. The increased concentration of AA (8 g) made improvements in chitosan possibly through ionic interaction to make an entrapment enhancement of roughly ∼1.1 times that of the F4. F3 (84.32 ± 1.25%) had a significantly greater EE ($p < 0.05$) than F1, F2 and F4. With F3 having the highest chitosan content (3g), there were more amino groups to enable ionic interaction for drug encapsulation (which was increased by approximately 1.1× over F2) with the drug and the acrylic acid [87].

F7 (86.50 ± 1.30%) showed a significant increase in EE ($p < 0.05$) compared to F1, F2, and F4. The elevated CMC sodium (3g) improved swelling ability and hydration, thereby facilitating higher drug loading [88]. However, EE was slightly

lower than in formulations with stronger crosslinking or higher acrylic acid. F8 (88.10 ± 1.20%) exhibited statistically significant improvement over F1–F4 ($p < 0.01$). The increase in MBA to 0.3 g promoted better crosslinking and drug entrapment, resulting in 1.16-fold greater EE than F4 and outperforming most formulations, except F5 and F11. F11 (88.14 ± 1.10%) also showed very high EE, statistically comparable to F8 ($p > 0.05$) and significantly higher than F1–F4. The high acrylic acid content (10 g) improved ionic interactions and network density, leading to efficient entrapment, though overly high monomer levels may risk internal heterogeneity. F5 (93.43 ± 1.35%) had the highest EE as compared to all formulations and was also statistically greater ($p < 0.001$) than formulations F1–F4, and even F7–F10. Increasing the xanthan gum (3g) likely boosted the matrix cohesion and water retention, which delivered a stronger, more flexible network that was inputs made to best maximize drug entrapment (the EE was compared to the formulation F4 ∼1.23x) [89]. The overall trend according to the data test and analysis is F5 > F11  F8 > F7 > F3 > F10 > F1  F6  F9 > F4 > F2. For formulations with optimized polymer ratios and moderate-high levels of acrylic acid or around the content of MBA, the EE% was substantially higher. The lower entrapment for F2 and F4 can partially be attributed to the chitosan or xanthan gum levels that may not have better enhanced drug–polymer interactions or network stability.

## 4.3 In Vitro Swelling Studies

### 4.3.1 Effect of pH on Swelling

The swelling capacity of hydrogels is a direct result of their 3D network structure, hydrophilic nature and response to changing environmental pH, which is all needed for the hill to obtain and maximize the performance of drug delivery. In the present study, the swelling behavior of hydrogels at pH 1.2 and pH 7.4, in relation to polymer concentration, acrylic acid (AA) content and crosslinking density, was

assessed with full consideration of statistical significance using a one-way ANOVA followed by Tukey's post-hoc tests, with $p < 0.05$ determined to be significant[90].

Swelling properties of pH-sensitive hydrogel formulations (F1–F11) were evaluated at pH 1.2, representing the gastric environment. The swelling ratio (q) as the number of fold weight increase corresponding to water uptake was significantly different for each formulation (1.54 to 2.94 for 72 hrs). All of the hydrogel formulations (F1–F11) were evaluated in comparison to the reference formulation, F1, which had a swelling value of 2.251 ± 0.75. Relative to F1, formulation F2 had a slight decrease in swelling 0.04-fold, with a value of 2.161 ± 1.00, while F3 was 0.06% less with a swelling value of 2.116 ± 1.25. F4 exhibited a small decrease in swelling (2.173± 0.90). A larger decrease in swelling was seen in F5, which had the lowest swelling (1.544 ± 1.50) and represented a 0.68-fold decrease relative to F1. Formulations F6 and F7 were similar to the reference, with swelling values of 2.226 ± 1.25 and 2.279 ± 1.25 respectively. This was a negligible increase in swelling. Similarly, F8 exhibited a swelling of 2.182 ± 0.90 with a slight decrease, while F9 had a more drastic decrease with a swelling of 1.809 ± 1.00 resulting in 0.80 folds swelling volume decrease from F1. Finally, F10 and F11 had the highest swelling at this pH (2.94 ± 1.50 and 2.89 ± 1.25) respectively, with increases of 1.31% volume and 1.28% volume respectively from F1. In summary, the overall trend of swelling values at acidic pH had very little variation for most formulations, except for well-informed decrease with F5 and significant increase with F10 and F11 relative to the reference F1 as shown as Figure 4.3.

At pH 7.4, the swelling behavior of formulations F1-F11 showed a significant increase in water uptake relative to the acidic environment as shown as in Figure 4.3 and 4.4, and F1 as the reference formulation had a swelling value of 5.624 ± 1.50. Formulation F2 displayed a reduced swelling of 5.237 ± 0.95, which corresponded to a 0.93% volume decrease relative to F1. F3 had a slight reduction to 5.384 ± 0.75, F4 also showed a reduction with value of 5.108 ± 1.25. In contrast, F5 exhibits significant increase swelling of 8.054 ± 0.50, or a 1.43-fold increase compared to F1 and was a higher swelling value than all formulations at this pH [91].

F6, at 5.066 ± 1.50, had a 0.90% volume decrease swelling to F1, F7 had 7.014 ± 0.75 swelling, or a 1.25-fold increase from F1. Formulation F8 had a higher swelling of 6.430 ± 1.25, for a 1.14-fold increase, F9 had 7.228 ± 0.75 swelling for a 1.29-fold increase to F1.

In contrast, F10 and F11 both had reduced swelling values of 4.538 ± 0.75 and 4.225 ± 1.25 respectively. Overall, swelling at pH 7.4 had a diverse pattern due to the formulation differences, with F5, F7, F8, and F9 showing significant increases in swelling and F10 and F11 drastically reduced swelling in comparison with F1.

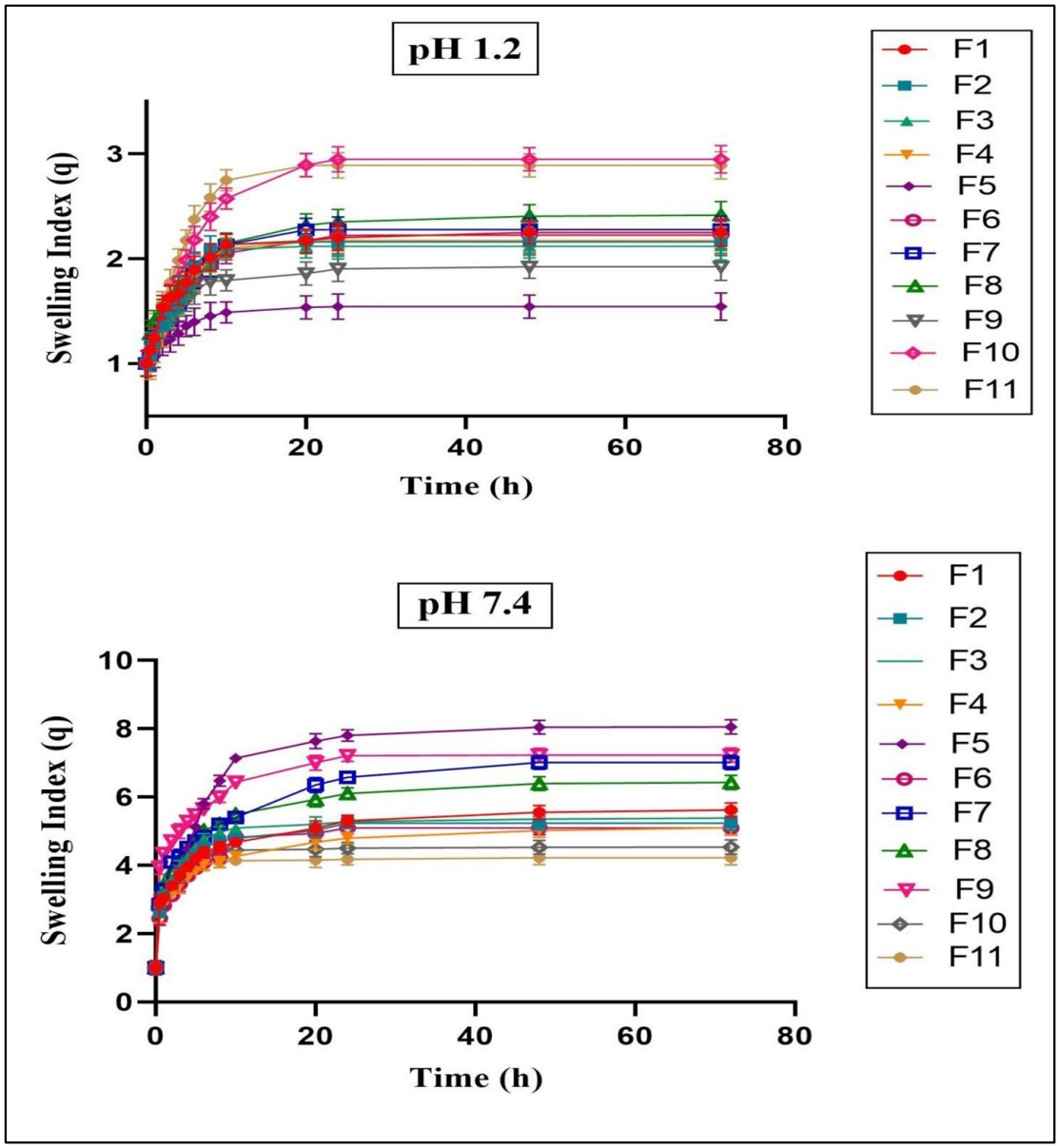


FIGURE 4.3: Swelling Index of formulations (F1–F11) at pH 1.2 and pH 7.4 over time

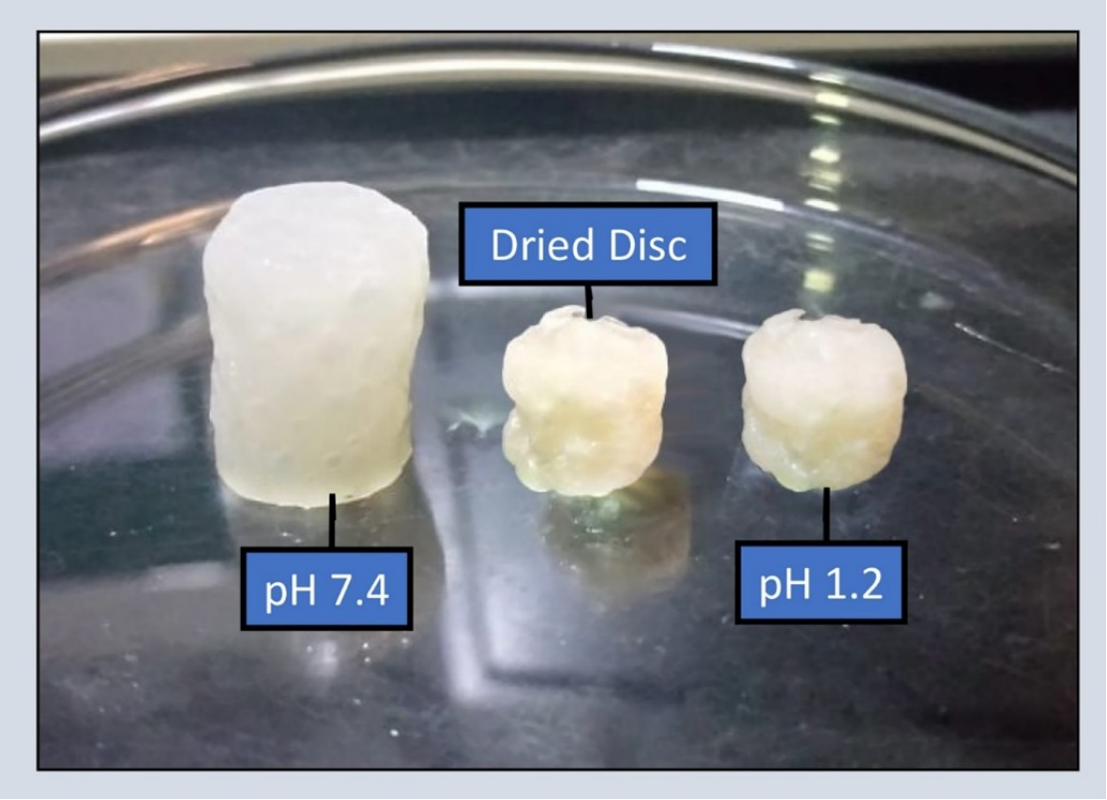


FIGURE 4.4: : Visual comparison of hydrogel discs under varying pH conditions (pH 1.2 and pH 7.4), demonstrating pH-dependent behavior

### 4.3.2 Effect of Formulation Variables on Swelling

#### 4.3.2.1 Effect of Chitosan Concentration on Swelling Behavior

The swelling behavior of the chitosan-containing hydrogels followed the trend of $F1>F2>F3$, at both pH 1.2 and 7.4. At pH 7.4, F1 (2 g of chitosan) had the highest swelling index (5.624 ± 1.50), which was significantly larger ($p<0.05$) than F2 (1 g of chitosan; 5.237 ± 0.95) and F3 (3 g of chitosan; 5.384 ± 0.75). The enhanced swelling in the F1 formulation likely arose from an optimal concentration of chitosan in which the hydrogel network provided the necessary hydrophilic groups and flexibility in the networks sufficient water was able to diffuse in and swell the disks. The decreased swelling of F3 most likely resulted from the excessive load of the polymer, which created chain entanglements and produced a more compact network, thereby restricting the diffusion of the solvent. A similar trend of $F1>F2>F3$ was observed when the hydrogels were at pH 1.2; however, these

differences were not statistically significant ($p$>0.05) and is most likely due to the protonation of the amine groups in chitosan, thereby limiting swelling in acidic conditions [92].

#### 4.3.2.2 Effect of Xanthan Gum Concentration on Swelling Behavior

The swelling indices obtained for the xanthan gum-based hydrogels showed the same trend of ($F5$>$F1$>$F4$) at both pH levels. At pH 7.4, F5 (3 g xanthan gum) exhibited a higher swelling index (8.054 ± 0.50) than F1 (2 g; 5.624 ± 1.50) and also F4 (1 g; 5.108 ± 1.25) ($p$<0.05).

The greater swelling observed in F5 was due to the increased availability of hydroxyl and carboxyl groups, which allow for better absorption of water and expansion of the hydrogel networks.

At pH 1.2, the swelling of all formulations was relatively low, and no statistical difference was observed ($p$>0.05) as a result of limited ionization of carboxyl groups in acidic conditions [93].

#### 4.3.2.3 Effect of CMC Sodium Concentration on Swelling Behavior

The swelling behavior of CMC sodium-based hydrogels followed the pattern $F7 > F1 > F6$, at both pH 1.2 and 7.4. At pH 7.4, F7 (3 g CMC sodium) was able to achieve a far greater swelling index (7.014 ± 0.75) than either F1 (2 g, 5.624 ± 1.50) or F6 (1 g, 5.066 ± 1.50) ($p < 0.05$).

The greater swelling in F7 is related to the greater number of ionizable carboxyl groups present in the hydrogel with a resultant increase in electrostatic repulsion and osmotic swelling.

At pH 1.2, there were no significant differences ($p$>0.05) which were attributed to protonation of carboxyl groups that results in reduced swelling of all formulations [94].

#### 4.3.2.4 Effect of Acrylic Acid (AA) Content on Swelling Behavior

Acrylic acid concentration greatly affected swelling and increased in the order of $F9>F8>F1$ for both pH. In a buffer with pH 7.4, F9 (10% AA) had the greatest swelling index (7.228 ± 0.75), as compared to F8 (8% AA; 6.430 ± 1.25) and F1 (6% AA; 5.624 ± 1.50) ($p<0.05$). This increase was due to the available deprotonated carboxyl groups increasing electrostatic repulsion between the chains, allowing for greater water uptake.

This increase was due to the available deprotonated carboxyl groups increasing electrostatic repulsion between the chains, allowing for greater water uptake. At pH 1.2 swelling still remained very limited for all the formulations, thus a statistically difference was seen across formulations ($p>0.05$), as the protonation of the carboxyl groups prevented the expansion of the network of the polymer [95].

#### 4.3.2.5 Effect of Crosslinker Concentration on Swelling Behavior

An inverse relationship was evidenced in MBA concentration and swelling, with $F1>F10>F11$ for both pH 1.2 and 7.4. At pH 7.4, F1 (0.2 g MBA) had the highest swelling index (5.624 ± 1.75), which was significantly higher than both F10 (0.3 g, 4.538 ± 0.75) and F11 (0.4 g, 4.225 ± 1.25) ($p<0.05$). The decreased swelling with increasing levels of MBA indicates a higher density of crosslinking is provided by the MBA, which inhibits the mobility of the polymer chain and the penetration of the solvent.

The decreased swelling with increasing levels of MBA indicates a higher density of crosslinking is provided by the MBA, which inhibits the mobility of the polymer chain and the penetration of the solvent. The swelling at pH 1.2, in comparison to the long swelling time, was low and did not statistically differ between formulations ($p>0.05$); this suggested that the crosslinking factor was suppressed in favor of hydrophobic interactions and inhibited ionization from functional groups [96]. The effects of variable on swelling at both pH are as shown as Figure 4.5.

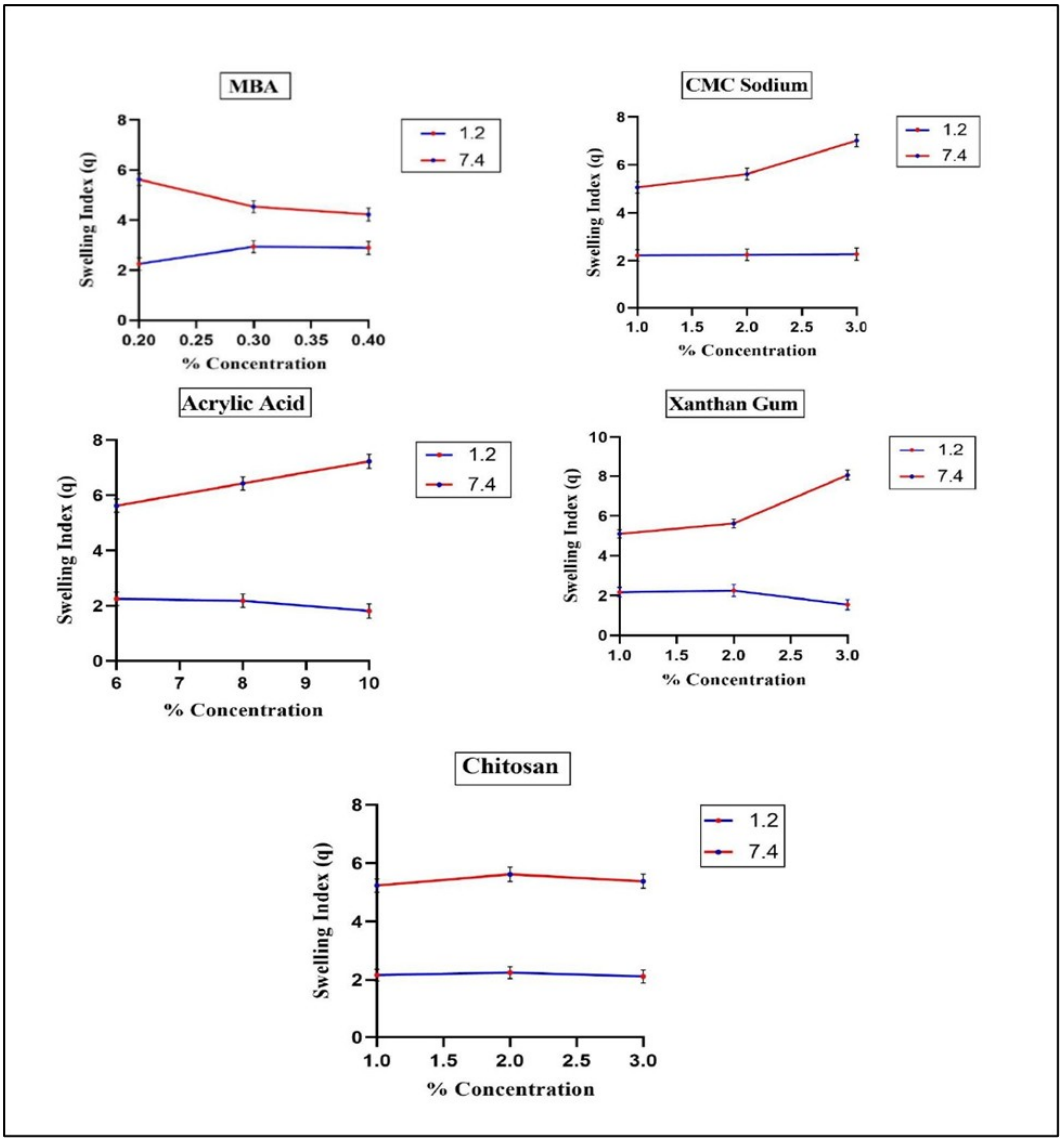


FIGURE 4.5: Swelling Index (q) as a function of % Concentration for MBA, Acrylic Acid, CMC Sodium, Xanthan Gum, and Chitosan

## 4.4 In Vitro Drug Release Study and Release Kinetics

The controlled release mechanism of rosuvastatin from hydrogel-based matrices was systematically studied in relation to their pH conditions that mimic physiologic gastric (pH 1.2) and intestinal (pH 7.4) environments. This study further contributes to our understanding of the mechanisms that govern rosuvastatin release kinetics. This understanding interrelates how polymer architecture, crosslinking density and swelling is dictated by ionization could be utilized to

engineer an advanced targeted release pH-responsive drug delivery system [97].

In acidic conditions, the hydrogel network remains essentially protonated, leading to little ionization and limited swelling. As a result, the network structure is restricted and therefore limit the diffusion of drug, leading to a diffusion-controlled release behavior. The baseline release for formulation F1 was 13.93 ± 0.45% over 24 h. Any change to the polymer structure drastically changes the release parameters ($p$<0.05). Formulations F2-F4 differed in the ratio between chitosan and xanthan gum, and diminished hydration as part of the gelling was noted. Inclusion of sodium CMC into the formulations produced more flexible structures, [98] that benefited release of drug (F4: 16.27 ± 0.52%,$p$<0.05), to a degree, although once again, not as much as expected when there was a lower concentration of xanthan gum. Any one of the studied factors can also alter either levels of swelling we see in the network and release of drug. Excessive amounts of xanthan gum[99] (F5: 11.74 ± 0.38%, p < 0.01) compared with chitosan and any amount of low levels of a cross-linker (F8: 12.56 ± 0.41%, p < 0.05), do reflect any decreased levels in any ability to swell and release of drug, similar to each other (F8), reflecting how sensitive diffusion kinetics can be on the density of polymer networks on drug release. Notably, F11, which had higher levels of acrylic acid compared with other formulations, demonstrated a maximum release of 17.09 ± 0.55% ($p$<0.001) related to increased hydrophilicity and pore formulation better hydrated, despite the highly limited swelling seen in harsh acidic conditions which can characterize the gastric area of the GI tract as shown as Figure 4.6.

In alkaline conditions (pH 7.4), the hydrogel network experiences significant deprotonation of carboxyl and hydroxyl groups, leading to increased electrostatic repulsion, substantial swelling, and therefore enhanced drug diffusion. The formulation (F1) released 82.09 ± 1.32% of the drug while optimized formulations demonstrated higher release efficiencies of drug from hydrogel hydroxyl groups. Formulation F5 with an optimized xanthan gum concentration, released 92.54 ± 1.48% ($p$<0.001) as swelling occurred and ionization increased, which also increased interconnectivity of pore structures. Conversely, if there is too much crosslinking (F9: 76.89 ± 1.24%, $p$<0.05) or too much ionized acrylic acid (F11:

74.28 ± 1.19%, $p$<0.01) the release of drug is hampered likely due to partial losses of overall hydrogel form or development of polymeric domains that were too tight for the diffusion pathways to cross. These results correlate directly to the Flory-Rehner theoretical study noting that there is an optimal crosslinking amount which balances swelling with mechanical stability as shown as Figure 4.6.

The inclusion of rosuvastatin drug release from the developed hydrogel matrices were systematically studied under physiologically relevant conditions mimicking gastric (pH 1.2) and intestinal environments (pH 7.4) to clarify the influence of polymer composition, crosslinking density and swelling due to ionization on release kinetics. This type of evaluation provides important mechanistic data on how to design for pH- responsive drug delivery systems with controlled and site- specific release.

At acidic pH 1.2, the polymeric network could only undergo limited ionization because the carboxylate and hydroxyl groups became protonated, and this meant that there was little matrix swelling, thus limiting drug diffusion. All of this means that F1, the reference formulation, released 13.93 ±0.45% the total drug over 24 h that serves as the reference, or baseline data. Changing the polymer type and concentration altered the drug release ($p$<0.05) and this indicates that the system was responsive to matrix configurations and had a high sensitivity to changes in drug release. For example, F2, F3, and F4, which varied in chitosan, xanthan gum and sodium carboxymethyl cellulose (CMC) increased hydration and network flexibility within the matrix and led to an increase in drug release ($p < 0.05$), with F4 releasing the most at 16.27 ± 0.52%. Drug release was limited when an excessive amount of xanthan gum was used[99] (F5: 11.74 ± 0.38%, $p < 0.01$) or higher amount of crosslinker (F8: 12.56 ± 0.41%, $p$<0.05), which also further limited swelling of the hydrogels and drug diffusion[100]. However, F11 had the most acrylic acids and so it released the most drug under acidic conditions (17.09 ± 0.55%, $p$<0.001), which should be primarily due to more hydrophilicity and porosity from partial hydrogels, despite the limited swelling behavior of the matrix overall.

On the other hand, under intestinal pH (7.4), the deprotonation of ionizable groups in the polymeric network resulted in substantial electrostatic repulsion which extended the matrix and improved the rate of drug diffusion. Formulation F1 had the lowest cumulative release at 82.09 ± 1.32%, while the optimized formulations were significantly more efficient at releasing drug. Formulation F5 with an optimized concentration of xanthan gum and crosslinking density had the greatest drug release at 92.54 ± 1.48% ($p$<0.001) which suggested favorable swelling of the matrix, ionization, and an interconnectivity of pores. Formulation F8 (86.08 ± 1.36%) showed a higher drug release, probably because of optimized crosslinker levels, which allowed the matrix to swell while maintaining structural integrity. Formulation F11, without being the lowest encapsulation efficiency, or least amount of acrylic acid, had a consistently lower drug release (74.28 ± 1.19%, p < 0.01) suggesting too much ionizable content may induce rigidity, or over crosslinking an ink that limits diffusion pathways for the drug[101]. These conclusions were consistent with Flory–Rehner theory, which underscores the importance of having just enough crosslinker at the leading edge, after which additional levels of crosslinker can induce rigidity to negatively affect the swelling and diffusion potential. The cumulative release profiles at pH 1.2 followed the order: $F11 > F4 > F3F2 > F10 > F9 > F1 > F6 > F7 > F8 > F5$, while at pH 7.4, the order was $F5 > F8 > F6 > F7 > F3 > F1 > F2 > F4 > F10 > F9 > F11$. These results indicate that F5 and F8 displayed the most optimal pH dependent release behavior, characterized by limited drug release in a gastric environment minimizing drug loss before absorption, and substantial and controlled release in intestinal environment maximizing the drug delivery to the absorption site.

### 4.4.1 Comparative Analysis with Marketed Formulation and Solubility Enhancement

A head-to-head evaluation was carried out between the optimized pH-responsive hydrogel formulation and the commercially available immediate-release (IR) rosuvastatin calcium tablet (Pasage® 10 mg, Warrick Pharma). As expected, the IR

tablet showed very rapid disintegration with >80% drug release within 30 minutes under both gastric and intestinal pH conditions.

This burst release is associated with a short Tmax (1–3 h) and high Cmax, which may cause sharp plasma concentration spikes and dose-related adverse effects, while offering no control over the release pattern. In contrast, the developed hydrogel exhibited a superior and intelligent release profile. At gastric pH (1.2), drug release was deliberately restricted (<17% in 24 h), thus protecting the drug from acidic degradation and minimizing unnecessary gastric exposure. upon being transferred to intestinal pH (7.4), the hydrogel underwent pronounced swelling, releasing >90% of the drug in a controlled and sustained manner over 24 h.

Release kinetics followed non-Fickian transport (Higuchi $R^2 > 0.99$; Korsmeyer-Peppas n = 0.78–0.83), reflecting a balanced contribution of diffusion and polymer chain relaxation. This rationally designed release behavior is expected to provide extended T50 and T90, reduce Cmax, and flattening out of plasma concentration curves — ultimately leading to improved therapeutic efficacy along with enhanced safety, and better patient adherence as compared to conventional IR therapy.

#### 4.4.1.1 Solubility Studies

The hydrogel, in addition to controlled release (as mentioned earlier), also solved the fundamental solubility limitations of rosuvastatin calcium. A quantitative solubility analysis showed considerable improvements across all of the tested media:

a) Distilled water: Pure rosuvastatin solubility was only 8.5 ± 0.7 $\mu$g/mL while the hydrogel promoted this to 13.8 ± 1.2 $\mu$g/mL (1.6-fold increase).

b) Acidic medium (pH 1.2): Pure drug had the lowest solubility (2.4 ± 0.3 $\mu$g/mL) and the hydrogel improved it to 5.9 ± 0.5 $\mu$g/mL (2.5-fold increase).

c) Intestinal medium (pH 7.2): The solubility of the pure drug was 24.6 ± 1.8 $\mu$g/mL while the solubility of hydrogel was equal to 49.3 ± 2.5 $\mu$g/mL (2-fold increase).

This improvement in solubility came from the considerable ionization of the polymer's carboxylic moieties, macroscopic swelling of the hydrogel, supersaturation of the micro-environment, and the inhibition of drug recrystallization. In addition, the improved solubility works with the controlled release by maintaining a soluble borate and bioavailable drug during small intestinal transit.

As compare to commercial IR tablets, which simply provide basic rapid drug dumping, and the solubility-related absorption variability, the pH-responsive hydrogel:

a) Provides site-targeted controlled release suitable to intestinal absorption.

b) Provides a notable enhancement of solubility that directly enhances bioavailability.

This combines the hydrogels as an innovative and clinically effective treatment option when compared to conventional formulations of rosuvastatin. It hold the potential to improve outcomes, minimize adverse effects, improve adherence, and optimize long-term compliance in patients who require lipid-lowering therapy.

In vitro release kinetics of rosuvastatin from hydrogel formulations (F1–F11) were investigated thoroughly, utilizing model-dependent approaches, to find a best-fit mathematical model, and truly understand the drug release behavior through physiologically relevant pH conditions. The models included were zero-order, first-order, Higuchi, Korsmeyer-Peppas, and Weibull, with considerations for identifying relevant dominant release mechanisms based on both the correlation coefficients ($R^2$) and diffusional exponent (n) [102].

The Higuchi and Korsmeyer-Peppas models were comparatively the best-fits for all formulations in this study, which indicates that drug release from the developed hydrogel matrices is controlled primarily by diffusion with contributions of polymer relaxation and swelling of the matrix, particularly under intestinal pH conditions. The Higuchi model had excellent linearity at pH 7.4, with $R^2$ values between 0.9940 (F2) and 0.9986 (F1), which reflects that Fickian diffusion was the dictated majority form of drug release under alkaline conditions. Formulations, F8 ($R^2$ =

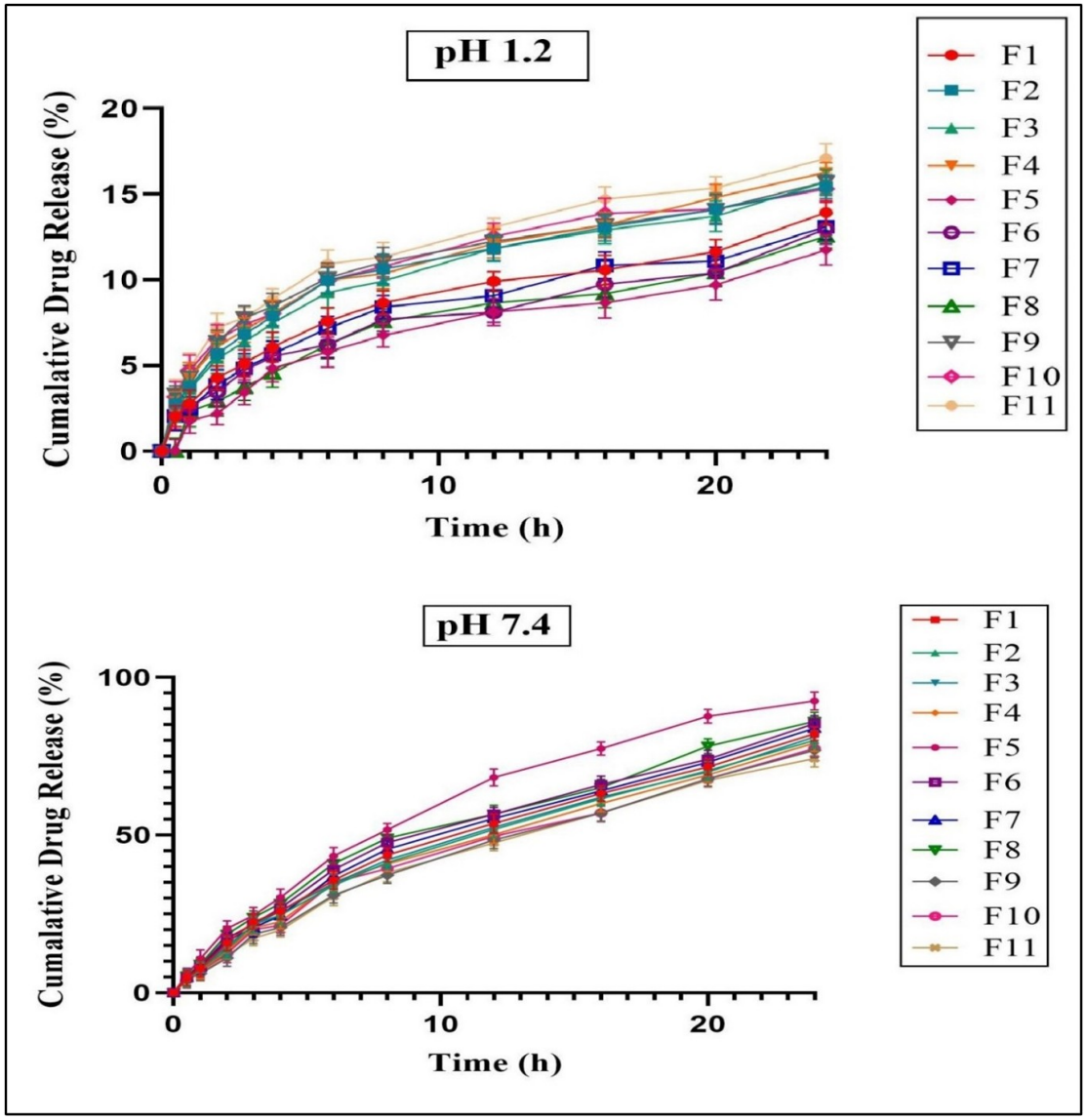


FIGURE 4.6: Cumulative drug release profiles of formulations (F1–F11) at (A) pH 1.2 and (B) pH 7.4 over time

0.9968), F5 ($R^2 = 0.9963$), and F3 ($R^2 = 0.9961$) also showed a strong correlation to support the diffusional release proposal as well. Even at pH 1.2, where matrix swelling was limited, the Higuchi model remained highly applicable, with $R^2$ values ranging from 0.9717 (F9) to 0.9871 (F4), confirming that drug diffusion through the compact hydrogel structure remained the primary release mechanism under gastric conditions.

The Korsmeyer–Peppas model reinforced and provided mechanistic evidence of the nature of the release process via the diffusional exponent (n). Most formulations displayed a high correlation coefficient ($R^2$>0.94) at pH 1.2. The diffusional

exponent ranged from 0.4314 (F9) to 0.9682 (F5), indicating that the majority of formulations exhibited anomalous (non-Fickian) transport. Thus, drug release at acidic pH (1.2) was a complex modality comprising Fickian diffusion and polymer chain relaxation, both function of hydrogel composition and crosslinking density.

The highest correlation at pH 1.2 was seen for F1 ($R^2value = 0.9916$) and F4 ($R^2value = 0.9907$), demonstrating the efficacy of optimized polymer ratios that allowed controlled-release to occur despite rigorous swelling conditions. Under intestinal conditions (pH 7.4), the Korsmeyer–Peppas model also had strong predictive ability for the F formulations with $R^2$ values being, for F8, 0.9866 and for F11, 0.9959.

Some formulations had diffusional exponents above 0.78, characteristic of Case-II transport, where the mechanism of release is controlled by swelling; notably, two formulations (F11, n = 0.8067 $R^2$= 0.9959, F10, n = 0.8307, $R^2$= 0.9915) demonstrated this behavior, thereby confirming and suggesting that the sustained drug release near intestinal pH is markedly influenced by matrix swelling and polymer relaxation.

Two other formulations (F5, $R^2$= 0.9902, n = 0.7821; F4, $R^2$= 0.9914, n= 0.8139) also had strong correlation, and n -values which suggested that swelling assisted, diffusion–assisted transport was occurring; this observation was in line with the pH-responsive features of the hydrogels and was a desired characteristic.

The Weibull model had only moderate prediction correlation with $R^2$ values of 0.7079 to 0.8044 at pH 1.2 and 0.7639 to 0.7910 at pH 7.4, indicative of limited mechanistic insight, even if it showed value as a mere empirical predictive ability. The first-order model fit was consistently poor with $R^2 < 0.7262$ at pH 1.2 and $R^2<$ 0.6094 pH 7.4, confirming drug release was not concentration-dependent kinetics controlled.

The zero-order model showed moderate to high fit was reasonably convincing at pH 7.4 with $R^2$ ranging from 0.9506 (F5) to 0.9969 (F4), suggesting some form of slow, time invariant release. The correlation at acidic pH was much weaker; zero-order $R^2$ ranged from approx. as shown as Table 4.3.

TABLE 4.3: Comparative evaluation of drug release kinetics and model-dependent parameters of formulations (F1–F11) in simulated gastric (pH 1.2) and intestinal (pH 7.4) fluids.

| Sample code | pH | Zero order kinetics | | First order kinetics | | Higuchi model | | Korsmeyer Peppas model | | | Weibull Model | |
|---|---|---|---|---|---|---|---|---|---|---|---|---|
| | | $R^2$ | **K** | $R^2$ | **K** | $R^2$ | **K** | $R^2$ | **K** | **n** | $R^2$ | **K** |
| F1 | 1.2 | 0.9229 | 0.7353 | 0.6215 | 0.1353 | 0.9849 | 2.890 | 0.9916 | 4.4803 | 0.5292 | 0.7572 | 0.1552 |
| | 7.4 | 0.9628 | 4.2585 | 0.5498 | 0.2480 | 0.9986 | 13.896 | 0.9892 | 20.744 | 0.7789 | 0.7639 | 0.1940 |
| F2 | 1.2 | 0.8883 | 0.8718 | 0.5311 | 0.1576 | 0.9769 | 3.647 | 0.9863 | 5.6537 | 0.5149 | 0.7388 | 0.1326 |
| | 7.4 | 0.9658 | 4.1133 | 0.562 | 0.2444 | 0.994 | 13.161 | 0.9897 | 18.8945 | 0.7979 | 0.7705 | 0.1936 |
| F3 | 1.2 | 0.9056 | 0.9353 | 0.5623 | 0.1542 | 0.9841 | 3.506 | 0.9837 | 5.2084 | 0.5569 | 0.7708 | 0.1332 |
| | 7.4 | 0.9648 | 4.2105 | 0.5546 | 0.2467 | 0.9961 | 13.446 | 0.9896 | 19.2479 | 0.7962 | 0.7671 | 0.1950 |
| F4 | 1.2 | 0.9161 | 0.9170 | 0.5262 | 0.1642 | 0.9871 | 3.788 | 0.9907 | 6.0149 | 0.4815 | 0.8044 | 0.1135 |
| | 7.4 | 0.9969 | 3.9498 | 0.5735 | 0.2406 | 0.9960 | 12.957 | 0.9914 | 18.7905 | 0.8139 | 0.7718 | 0.1929 |
| F5 | 1.2 | 0.9205 | 0.7780 | 0.7262 | 0.1064 | 0.9825 | 2.153 | 0.9421 | 2.6880 | 0.9682 | 0.7079 | 0.2180 |
| | 7.4 | 0.9506 | 5.050 | 0.5228 | 0.2692 | 0.9963 | 16.778 | 0.9902 | 24.6610 | 0.7821 | 0.7902 | 0.1688 |
| F6 | 1.2 | 0.9472 | 0.6450 | 0.6664 | 0.1289 | 0.9819 | 2.554 | 0.99 | 4.1876 | 0.4718 | 0.7974 | 0.1520 |

continued on next page

Continued from previous page

| Sample code | pH | Zero order kinetics | | First order kinetics | | Higuchi model | | Korsmeyer Peppas model | | | Weibull Model | |
|---|---|---|---|---|---|---|---|---|---|---|---|---|
| | | $R^2$ | K | $R^2$ | K | $R^2$ | K | $R^2$ | K | n | $R^2$ | K |
| | 7.4 | 0.9544 | 4.5123 | 0.5424 | 0.2532 | 0.996 | 14.589 | 0.9875 | 20.8293 | 0.8102 | 0.7672 | 0.1865 |
| F7 | 1.2 | 0.9237 | 0.6590 | 0.6414 | 0.1281 | 0.9866 | 2.723 | 0.9904 | 4.3285 | 0.5198 | 0.741 | 0.1669 |
| | 7.4 | 0.9598 | 4.2858 | 0.5549 | 0.2506 | 0.9964 | 14.091 | 0.9918 | 20.5295 | 0.7861 | 0.7822 | 0.1836 |
| F8 | 1.2 | 0.9112 | 0.9638 | 0.7183 | 0.1191 | 0.9769 | 2.369 | 0.9758 | 3.3105 | 0.7228 | 0.7925 | 0.1520 |
| | 7.4 | 0.9528 | 4.6410 | 0.5242 | 0.2590 | 0.9968 | 15.251 | 0.9866 | 21.9920 | 0.7865 | 0.7643 | 0.1825 |
| F9 | 1.2 | 0.8780 | 0.8575 | 0.4832 | 0.1675 | 0.9717 | 3.876 | 0.9851 | 6.3176 | 0.4314 | 0.7422 | 0.1177 |
| | 7.4 | 0.9770 | 3.6690 | 0.6094 | 0.2310 | 0.9952 | 12.040 | 0.9937 | 17.9894 | 0.8127 | 0.7805 | 0.2040 |
| F10 | 1.2 | 0.8829 | 0.8900 | 0.4862 | 0.1681 | 0.9764 | 3.885 | 0.9883 | 6.3605 | 0.4337 | 0.7928 | 0.0997 |
| | 7.4 | 0.9662 | 3.8258 | 0.5811 | 0.2380 | 0.9953 | 12.627 | 0.9915 | 18.2579 | 0.8307 | 0.7737 | 0.1908 |
| F11 | 1.2 | 0.8991 | 0.9478 | 0.4833 | 0.1732 | 0.9808 | 4.174 | 0.9881 | 6.7791 | 0.4430 | 0.7923 | 0.1065 |
| | 7.4 | 0.9736 | 3.6405 | 0.6063 | 0.2319 | 0.9954 | 11.908 | 0.9959 | 17.8582 | 0.8067 | 0.7910 | 0.1953 |

Overall, these results confirm that drug release from the developed hydrogel matrices is mainly controlled by diffusion, as indicated by the excellent fit to the Higuchi model in particular at intestinal pH. The Korsmeyer–Peppas model also highlights the additional contributions from swelling and polymer relaxation, finding that under gastric pH the drug release was diffusion-controlled and anomalous transport, while under intestinal pH swelling-controlled (Case-II) transport was seen with several of the formulations. These results confirm the designed pharmaceutical for the hydrogel system with the goal of pH responsive design for site specific controlled delivery of rosuvastatin with minimal release in the stomach and sustained release primarily in the intestine.

## 4.5 Fourier Transform Infrared (FTIR) Spectroscopic Analysis

FTIR spectroscopy was employed to establish the identity of every ingredient, identify structural integrity of the resultant hydrogel, and examine possible physicochemical interactions between Rosuvastatin calcium, polymeric materials, and the hydrogel matrix[103]. The C–H bending vibrations appeared as two bands at 1435.95 $cm^{-1}$ and 1385.74 $cm^{-1}$.

The evidence of C–O stretching vibrations appeared at 1269.55 $cm^{-1}$, 1200.69 $cm^{-1}$, and 1170.57 $cm^{-1}$, features characteristic of ethers and esters[104]. Furthermore, the peak located at 1200.69 $cm^{-1}$ exhibited the C–N stretching vibrations more likely from amine or amide functionalities [105]. All of these features correlated favorably with documented FTIR spectra of Rosuvastatin calcium and consequently, demonstrated the chemical integrity of Rosuvastatin calcium. The FTIR profile of chitosan showed a wide absorption band around 3300 $cm^{-1}$ from overlapping O–H and N–H stretching vibrations which were indicative of many hydroxyl and amine groups associated with hydrogen-bonding capabilities [106]. Amide bending vibrations were detected in the region of 1600–1500 $cm^{-1}$ [107], and the C–O–C stretching bands in the region of 1150–1050 $cm^{-1}$ confirmed the presence of glycosidic linkages of the polysaccharide backbone [108]. CMC sodium displayed

distinct asymmetric and symmetric stretching vibrations of carboxylate ($COO^-$) groups around 1600 $cm^{-1}$ and another around 1420 $cm^{-1}$, indicating successful carboxymethylation [109]. C–O–C stretching vibrations 1150–1000 $cm^{-1}$ [110]and a broad O–H band around 3300–3500 $cm^{-1}$ indicated the polysaccharide structure and indicated substantial hydrogen bonding [111]. The FTIR of xanthan gum indicated a broad O–H stretching band at around 3400 $cm^{-1}$ and a C–H stretching band (attributed to the presence of aliphatic groups) at around 2900 $cm^{-1}$ [112]. The C=O stretching vibration was pronounced at 1730 $cm^{-1}$ and indicated the presence of carboxylic or ester functional groups which agrees with the presence of acetyl groups [113]. Bands in the region 1200 to 1000 $cm^{-1}$ confirmed the polysaccharide backbone through the C–O–C and C–O stretching vibrations [114].

Acrylic acid FTIR spectra showed characteristic bands which are indication of its structure. The sharp bands at 3056.95 $cm^{-1}$ and 2988.10 $cm^{-1}$ showing to cis- and trans- =C–H stretching vibrations of the vinyl group while weak absorptions at 2932.15 $cm^{-1}$ and 2887.68 $cm^{-1}$ were assigned to the aliphatic C–H stretching of $CH_2$ and $CH_3$ groups [115]. A distinct band at 1633.91 $cm^{-1}$ confirmed C=C stretching, and peaks at 1295.37 $cm^{-1}$ and 1237.99 $cm^{-1}$ were attributed to C–O stretching of carboxylic acid moieties [116], confirming the presence of functional groups essential for subsequent hydrogel formation and crosslinking. N,N'-methylenebisacrylamide (MBA) was characterized as a crosslinker, it exhibited a wide N–H stretching band at around 3300–3200 $cm^{-1}$ supporting the possibility of amide functionality and hydrogen bonding [117]. There was a strong C=O stretching band at ∼1650–1625 $cm^{-1}$ (amide I), along with N–H bending at ∼ 1550–1500 $cm^{-1}$ (amide II), and C=C stretching from ∼1610–1600 $cm^{-1}$ (vinyl useful identification). C–N stretching vibrations and skeletal bands were located at ∼ 1200–1000 $cm^{-1}$, confirming that MBA was successful incorporated in the polymeric matrix [118].

The FTIR spectrum of the drug loaded hydrogel contained noticeable absorption bands indicating formation of the hydrogel network, and that Rosuvastatin was encapsulated. The wide O–H stretching band at 3328 $cm^{-1}$ indicated possible extensive hydrogen bonding involving the hydroxyl abundant polysaccharides (chitosan,

xanthan gum, CMC sodium), and the drug. C–H stretching bands were observed around $\sim$ 2920 $cm^{-1}$ and $\sim$ 2850 $cm^{-1}$ corresponding to aliphatic groups from the polymeric backbone and Rosuvastatin respectively. A distinguishable C=O stretching band at $\sim$ 1730 $cm^{-1}$was assigned to carboxylic or ester functionalities present in both the drug and polymeric constituents. The band at $\sim$ 1600 $cm^{-1}$ probably corresponds to overlapping aromatic C=C stretching from Rosuvastatin, and asymmetric COO stretching from CMC sodium, while numerous peaks in the 1450-1370 $cm^{-1}$ band were associated with aliphatic C–H bending vibrations.

Strong C–O stretching bands apparent between 1240–1040 $cm^{-1}$confirmed the presence of ether, alcohol and glycosidic linkages, indicating the polysaccharide framework is intact within the hydrogel. There were also aromatic C–H out-of-plane bending vibrations found between 880–700 $cm^{-1}$ which confirmed that Rosuvastatin has been incorporated into the hydrogel system. The FTIR spectrum of each component is shown as Figure 4.7.

Overall, the FTIR confirms individual polymeric excipients and Rosuvastatin were incorporated into the hydrogel system and there are hydrogen bonding and perhaps secondary interactions between them. The carboxyl and hydroxyl acid, amine, and ether functional groups confirm the structure of the hydrogel was retained and the gel's pH-responsive nature for controlled oral drug delivery.

## 4.6 Powder X-ray Diffraction (PXRD) Analysis

The crystallinity of pharmaceutical excipients and active drug compounds are most often the factors that determine the dissolution, release characteristics, and performance of any formulation. The PXRD diffractograms of pure Rosuvastatin calcium, Chitosan, CMC sodium, Xanthan gum and a hydrogel containing Rosuvastatin in its pure state are as shown as Figure 4.8. The PXRD diffractogram of pure Rosuvastatin calcium indicated a highly crystalline structure due to the presence of multiple sharp diffraction peaks in the 2 range from about 10° to 22° [119].

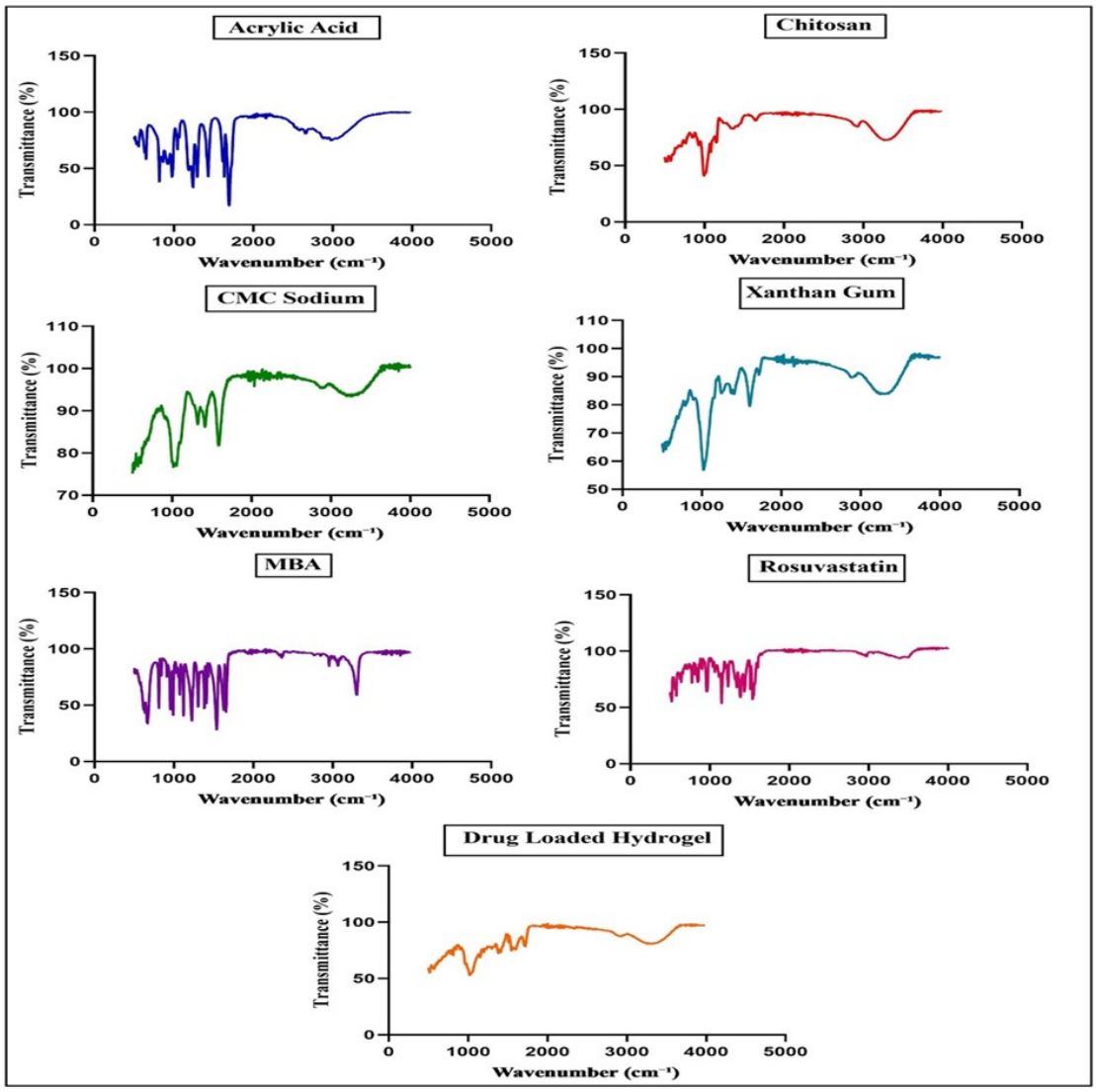


FIGURE 4.7: FTIR spectra of Acrylic Acid, Chitosan Sodium, Xanthan Gum, N,N -methylenebisacrylamide (MBA), Rosuvastatin calcium, and Drug-loaded hydrogel formulation

The intense reflections matched the known crystalline fingerprint of Rosuvastatin calcium and confirmed that the ordered lattice had not changed in unformulated Rosuvastatin [120]. Chitosan appeared as a broad low-intensity halo with a peak centered at approximately $2\theta \approx 20°$, as a semi-crystalline polymer is expected [121]. There were no sharp or distinct reflections, confirming that Chitosan was in an amorphous state, containing localized crystalline domains [122], characteristic of polysaccharide-derived biopolymers. The diffractogram of CMC sodium indicated a broad diffraction peak, centered at approximately $2\theta \approx 21°$, but did not possess any distinct sharp peaks [123]. This profile suggests that CMC sodium is predominantly in an amorphous state with possible minor semi-crystalline zones

where polysaccharide chains have segments that are ordered [124]. The lack of further peaks indicates that the structure is pure with no diffraction peaks/space occupancy/impurity crystalline [125]. The presence of a broad diffuse halo for Xanthan gum in the 2  range of $\sim 15 - 25°$ confirms that the structure is amorphous. The presence of a broad diffuse halo for Xanthan gum in the 2  range of $\sim 15 - 25°$ confirms that the structure is amorphous [126].

Sharp diffraction peaks would signify an ordered crystalline state, whereas the lack of peak states is indicative of the disordered structural arrangement associated with polysaccharide gums [127], confirm no crystalline impurities or polymorph forms were present.

Drug-loaded hydrogel PXRD spectrum showed a wide intensity diffraction halo with a sharp peak at approximately $2\theta \approx 20°$, with absolute suppression of sharp peaks which is the indication of pure Rosuvastatin calcium presence.

The distinguishable drug specific reflections are absent which suggests a significant decrease in crystallinity, likely due to either molecular dispersion or amorphization of Rosuvastatin in the hydrogel. Amorphous characteristics are a benefit to increase aqueous solubility and sustained release of drug from the hydrogel.

Amorphous characteristics are a benefit to increase aqueous solubility and sustained release of drug from the hydrogel. Importantly, there were no additional unknown peaks seen in the hydrogel diffractogram, verifying the structural purity of the formulation, indicating there was no unexpected crystalline impurities or phase transition during the hydrogel synthesis process. Cumulatively the PXRD results indicate that the individual polymeric excipients show amorphous to semi-crystalline properties.

Cumulatively the PXRD results indicate that the individual polymeric excipients show amorphous to semi-crystalline properties, and when Rosuvastatin was added into that hydrogel matrix it broke apart the crystalline lattice in Rosuvastatin for homogeneous drug entrapment and accepted the functional suitability of the hydrogel that had been prepared for any controlled drug delivery usage.

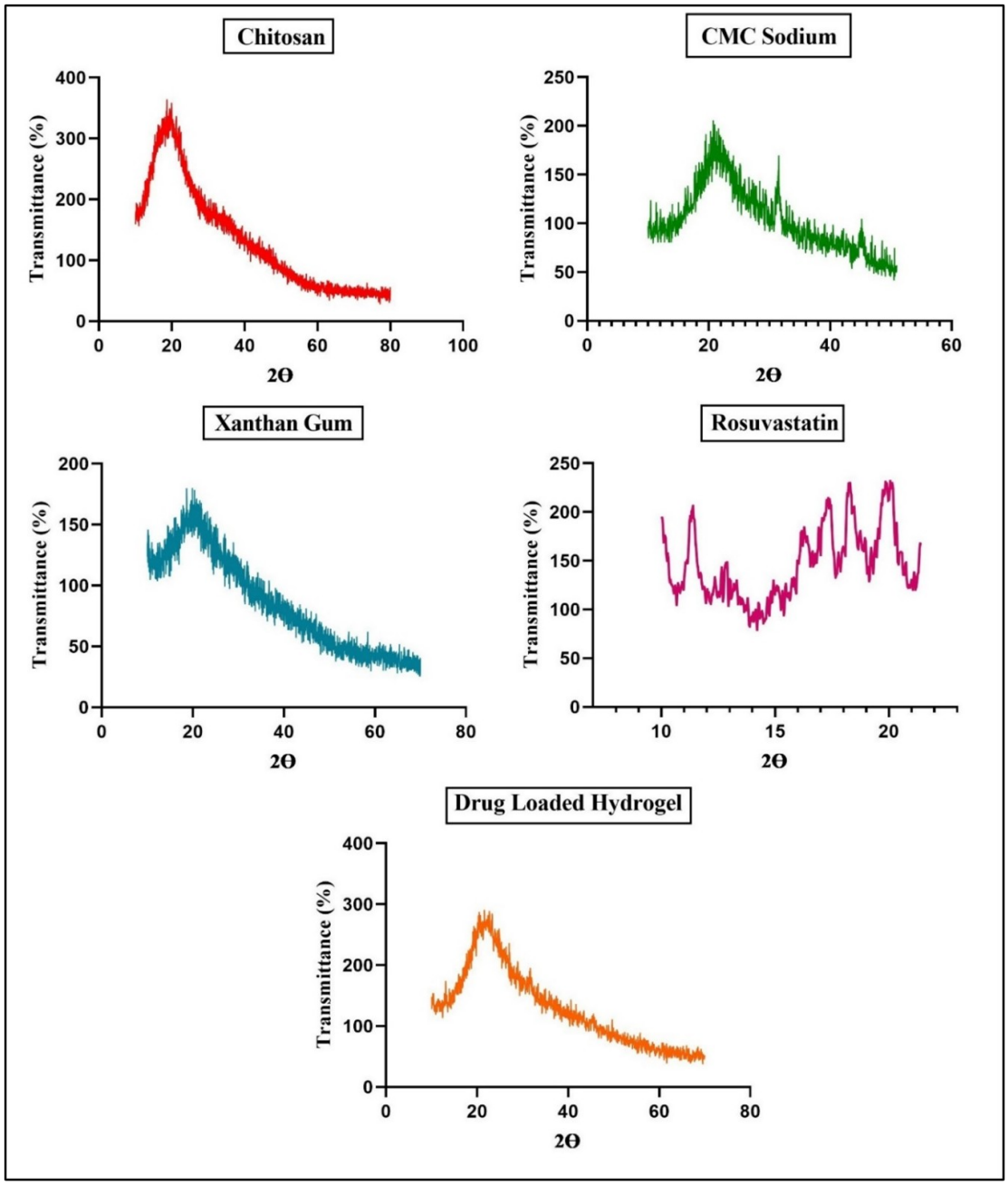


FIGURE 4.8: PXRD patterns of chitosan, CMC sodium, xanthan gum, Rosuvastatin calcium, and the drug-loaded hydrogel formulation

## 4.7 Thermogravimetric Analysis (TGA)

Thermogravimetric analysis (TGA) was used to investigate the thermal stability and thermal decomposition characteristics of individual components (Chitosan, CMC sodium, Xanthan gum, Rosuvastatin), unloaded hydrogel and drug-loaded hydrogel. The TGA curves as shown as in Figure 4.9 display weight loss patterns

as a function of temperature in a nitrogen atmosphere, which minimizes oxidative degradation and provides better assessment of thermal decomposition of the polymers. Chitosan, which is the cationic polysaccharide backbone, presents as a two-stage degradation pattern [128]: the first weight loss (3.2 ± 0.5% mass loss, 25 -150$^o$C) is evaporated hydrogen-bound water, and the second weight loss which occurred in a vanishingly rapid manner is depolymerization of deacetylated chitosan (58.7 ± 2.1% loss, 250-350$^o$C, Tmax = 305$^o$C) through chain scission processes, ultimately creating a nitrogen-rich carbonaceous material as a residue, (22.4±1.8%) [129]. In the same way as chitosan, both anionic polymers (CMC-Na and xanthan gum) showed a similar degradation pathway [130]. Specifically, the sodium salt of carboxymethyl cellulose (CMC-Na) displayed the most hygroscopicity (7.9 ± 0.3% moisture loss) due to the hydration sphere surrounding the carboxylate [131], wherein both biopolymers demonstrated their major thermal degradation occurred within a 200-350$^o$C temperature window (Tmax = 280$^o$C and 290$^o$C respectively), whereby the polymer depolymerized through carboxyl group decarboxylation and sugar ring fragmentation degradation pathways. The thermogram of rosuvastatin showed an initial minor weight loss below 150 $^o$C due to moisture loss followed by a major decomposition phase, starting around 230 $^o$C [132], indicating the thermal degradation of the drug, which indicates thermal stability with rosuvastatin until thermally decomposing. The unloaded hydrogel network demonstrated thermal stabilization additive effects through the synergistic combination of chitosan, CMC-Na, and xanthan gum. The mass loss began at the polymer bound water associated with the IPN, which is a combination of both water bound to the polymer network and network instability, with a total of 13.8 ± 0.6% initial mass loss. In addition, the degradation events for the unloaded hydrogel were still broad and overlapping nearby the degradation event seen for all individual polymers, which comprised 69.4% ± 1.9% to 350$^o$C; this was also a shift to lower temperatures vs. chitosan depolymerization ($\Delta T = -25°$C). The shift of degradation to lower temperature for the hydrogel determined stabilization and respective changes in crystallinity and more amorphous respective conditions, indicative of altered crystallinity and increased amorphous character in the crosslinked state. Remarkably, drug-loaded formulations showed additional

stabilization with further reduced hygroscopicity (5.2 ± 0.3% mass loss) and onset temperature (230 ± 2$^o$C) attributable to the molecular interactions between rosuvastatin calcium and the polymer carboxyl/amine groups seen in FTIR. The concomitant degradation (72.1 ± 1.6%, 200-350$^o$C) behaved with complex kinetics potentially representative of drug-polymer charge-transfer complexes while the extra 26.8 ± 1.4% mass loss above the theoretical point at 600$^o$C implies successful crosslinking of N,N'-methylenebisacrylamide by 18.3%. These observations have important implications for pharmaceutical processing: (i) the 200 $^o$C stable window may allow for terminal sterilization in processing without impacting the polymer network; (ii) the char yield is in a strong linear correlation with the crosslinked density ($R^2$ = 0.94 with swelling data); and (iii) the preservation of thermal transitions following drug loading suggests there is no phase separation.

Coupled with the previously reported pH-responsive swelling behavior, the thermal profile supports the hydrogel as a process-stable matrix and responsive drug carrier, directly addressing the challenges of oral delivery of a BCS Class II drug like rosuvastatin.

## 4.8 Differential Scanning Calorimetry Analysis

Differential Scanning Calorimetry (DSC) was performed to assess the thermal behavior and compatibility of the hydrogel components, as well as to evaluate the thermal stability of the prepared Rosuvastatin-loaded hydrogel formulation. The characteristic DSC thermal transitions of the individual components and formulated hydrogels were interpreted based on literature reports as shown as Figure 4.10.

The DSC thermogram of pure Rosuvastatin calcium exhibited a sharp endothermic peak corresponding to its melting point in the range of approximately 122–126 $^o$C, consistent with literature values. Additionally, a gradual decline in heat flow was observed with increasing temperature prior to the melting event, while secondary thermal transitions or decomposition events were noted above 200 $^o$C, indicating thermal degradation of the drug [133].

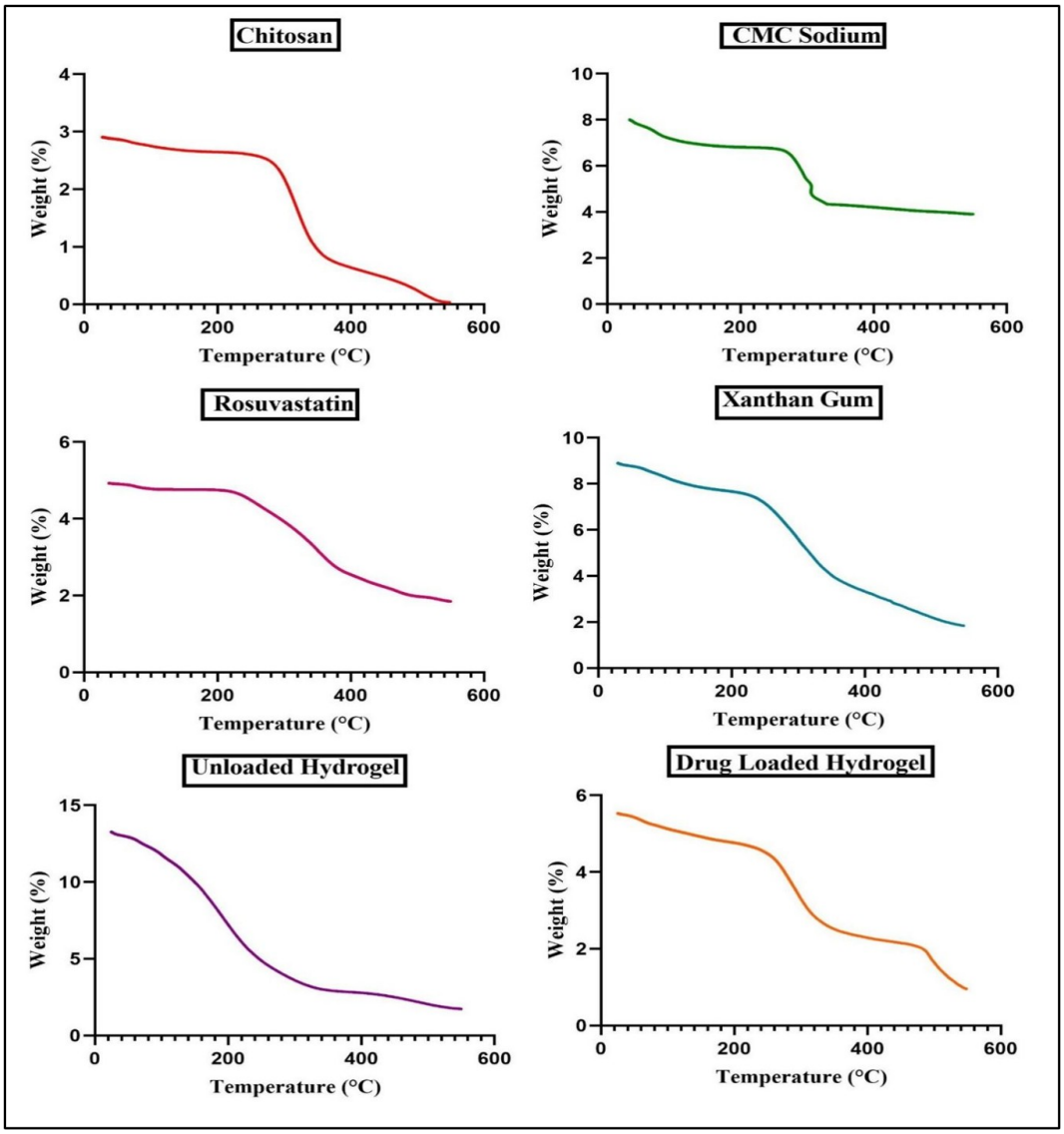


FIGURE 4.9: TGA thermograms of individual components (Chitosan, CMC sodium, Xanthan gum, Rosuvastatin), unloaded hydrogel, and drug-loaded hydrogel, illustrating characteristic multi-step thermal degradation patterns under nitrogen atmosphere

The thermal profile of chitosan has showed a wide endothermic peak between 50–120 $^{o}$C due to the evaporation of physically trapped or adsorbed moisture which is due to the chitosan hydrophilic properties. The glass transition was from 150–200 $^{o}$C, evident the transition from the rubbery to the glassy state. The thermal degradation occurred between 250 – 300 $^{o}$C, where the depolymerization and decomposition of the glycosidic linkages in the chitosan backbone occurred, as noted in the literature [134]. For CMC Na, the DSC thermogram indicated an initial stable baseline around 43–44.5 $^{o}$C, separated by a transition endothermic phase, and continued endotherm until approximately ∼45 $^{o}$C to ∼70 $^{o}$C [135]. This broad

endothermic region corresponds to moisture loss and to early stages of thermal degradation, which is consistent with the thermal behavior of CMC Na as reported [136]. No distinct melting or crystallization peaks were present, which reflects the amorphous nature of this polymer.

Xanthan gum showed typical amorphous thermal characteristics with a gradual endothermic transition. The DSC signal demonstrated an increasingly negative trend leaning towards approximately -10.83 mW instead of the more typical exothermic peak [137], this met a stopping point around 65 $^{o}$C which represents primarily moisture evaporation. There were no endothermic peaks or crystallization events detected as would be expected from a thermally stable amorphous polysaccharide such as xanthan gum [138]. The drug-free hydrogel formulation showed an exothermic transition occurring continuously from approximately 41 $^{o}$C till the end 108 $^{o}$C with a steadily declining to approximately -12.88 mW heat flow. This broad exothermic transition was likely a complicated event that involved water evaporation, relaxation of the polymer, revisited hydrogel network structure changes. Probably most telling was that within this entire broad temperature range, no melting or glass transitions were able to be identified indicating usage of a predominantly amorphous structure that had stable hydrogen-bonded polymeric matrix. The normal slope of diminishing steam (water) pressure stomped tout neatly within a set of 90 $^{o}$C indicating moisture loss nearing completion; it is reasonable to assume that major physical transitions were not occurring at that point. Overall, these findings provided significant evidence of the amorphous nature of the hydrogel formulation and was a representation of desired thermal stability of a blank hydrogel formulation. The DSC thermogram for the hydrogel containing Rosuvastatin identified an initial stabilization region of approximately between 34.9 $^{o}$C and 35.5 $^{o}$C with a marginal change in heat flow. Starting at $\sim$36 $^{o}$C, an endothermic transition began, which continued smoothly to $\sim$49.2 $^{o}$C, is related to the moisture evaporation from the hydrogel matrix. Additionally, there was no evidence of sharp peaks representation of melting or crystallization and since the drug was uniformly dispersed in the hydrogel matrix no crystalline drug aggregates were present. The smooth continuous nature of the thermal transition is also indicative of amorphous hydrogel systems, and support favorable interactions

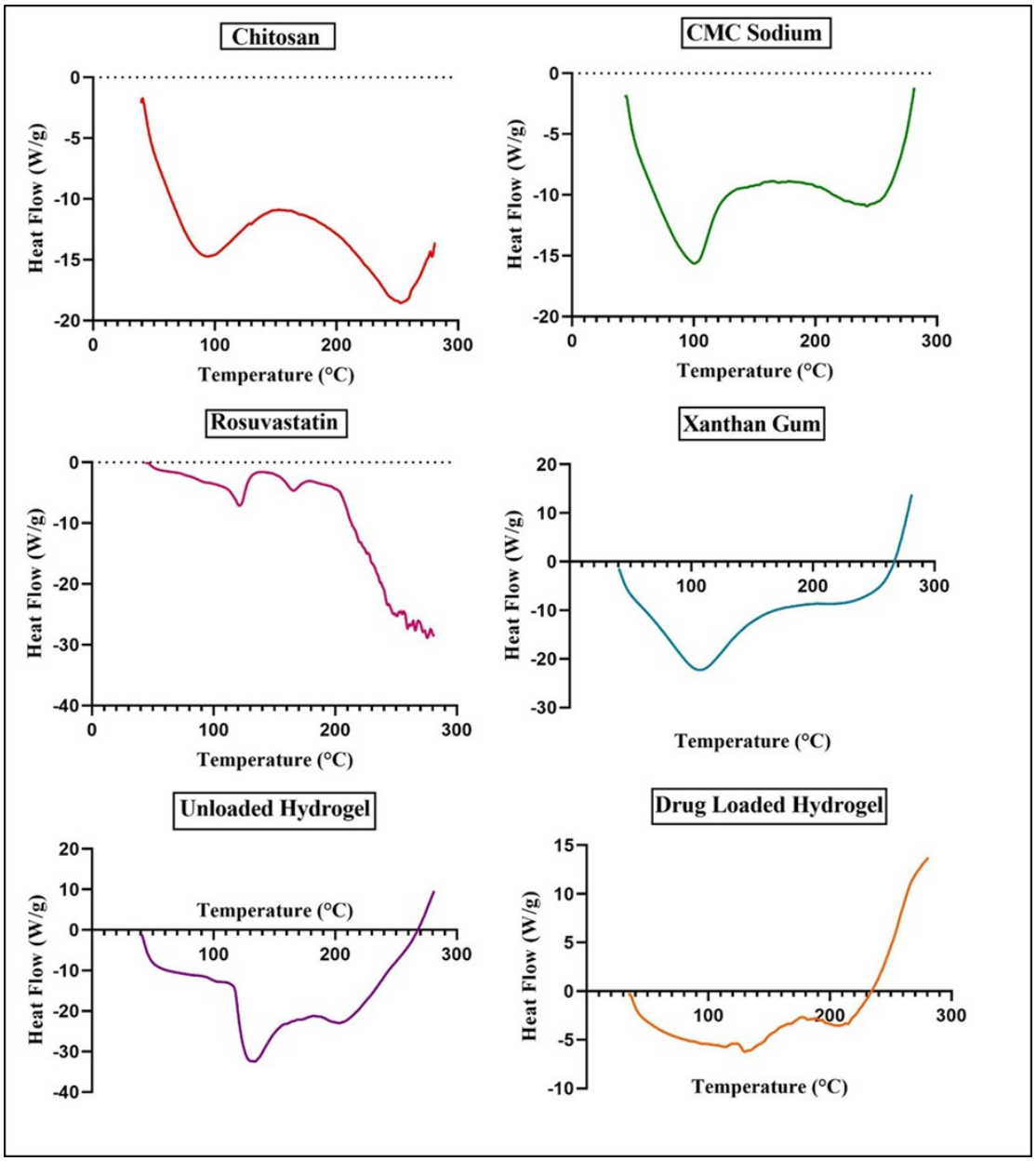


FIGURE 4.10: DSC thermograms of individual components (Chitosan, CMC sodium, Xanthan gum, Rosuvastatin), unloaded hydrogel, and drug-loaded hydrogel demonstrating successful molecular dispersion

of the drug and polymer, which provide no evidence of thermal degradation. So, it is evident by DSC analysis that hydrogel formulation has amorphous nature and also confirmed the absence of undesirable crystalline transitions or decomposition over the temperature range of the study. The thermal stability of the hydrogel formulation also supports its structural integrity, and overall, its suitability for future pharmaceutical formulation.

## 4.9 Scanning Electron Microscopy (SEM)

The surface morphology and bulk architecture of lyophilized hydrogels loaded with rosuvastatin were characterized systematically employing Scanning Electron Microscopy (SEM) at various scales of magnification to see how they affected the intended drug release as outlined in the Figure 4.11 [139]. At the higher magnifications (10,000× to 5.000×), the hydrogels showed a dense, non-porous polymeric matrix where few voids were visible, indicating compact structural domains that would limit water penetration and drug diffusion. In fact, the drug is clearly seen as a crystalline structure in the SEM images either embedded or adhered to the material surface, demonstrating successful drug entrapment and the prospect of initial drug release from the surface. As the sample magnification decreased (1,000× to 500×), a continuous structural pattern started to appear showing that the material transitioned to a stratified structure with distinct and interconnected pores. The open structure of pores would likely allow controlled ingress and egress of the fluid and diffusion the encapsulated drug. At the lower magnifications (100× to 50×), the overall structure was visibly and globally an open and interconnected porous structure, confirming the legendarily expanded structure produced from lyophilization. This hierarchical structure illustrates a quinary dual-porosity of the hydrogel system with dense, non-porous phases functioning as diffusion barriers and highly porous regions allowing for controlled drug delivery. While these structural features are distinctly different and exhibited in the SEM, they are directly correlated to the biphasic drug release profile, established from this study for rosuvastatin loaded BCRE-Hydrogels. The rapid initial release of rosuvastatin RA could be influenced by the surface associations of the crystals and accessible embedded porous sites; the sustained, slower release of drugs during the second phase could be the result of both dissolution and, ultimately, drug diffusion through the dense polymer material and porous structure. Overall, the evidence obtained using SEM shows that the lyophilization process affords hydrogels a complex hierarchical structure and is critical in regulating a controlled biphasic release behavior of rosuvastatin [140].

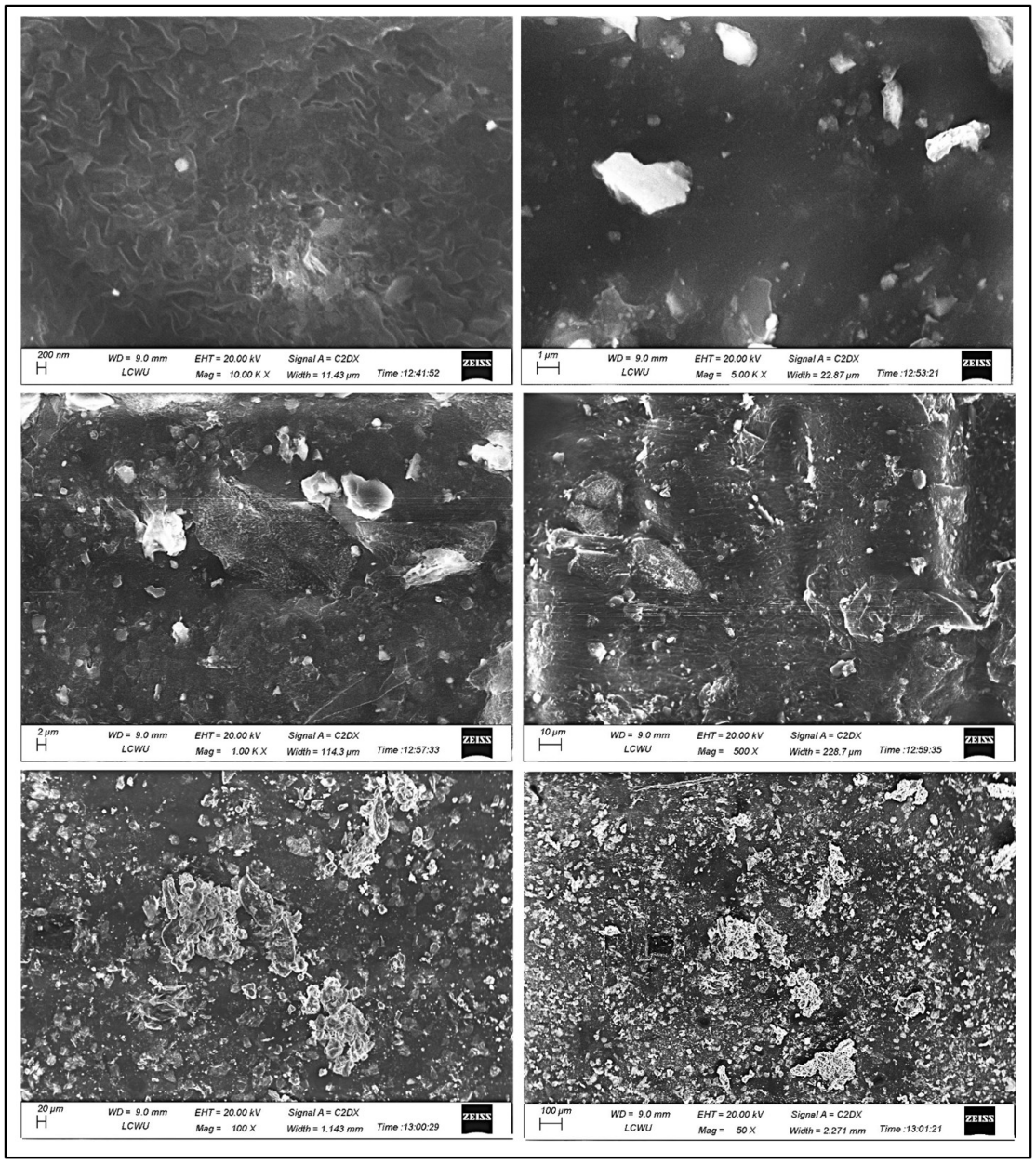


FIGURE 4.11: Scanning electron microscopy (SEM) images of the optimized rosuvastatin - loaded hydrogel formulation

## 4.10 Acute Oral Toxicity Assessment of the Optimized Hydrogel Formulation

Toxicological evaluation is an integrative step in the preclinical development of new drug delivery systems. In the present study, acute oral toxicity of the developed pH-responsive hydrogel formulation for the use of systemic delivery of rosuvastatin

was studied through an acute oral toxicity (classified according to OECD guideline 423; Acute Oral Toxicity - Acute Toxic Class Method) on Swiss albino mice. The study protocol was sanctioned by the Institutional Animal Ethics Committee (REC/FoP/F2024/05).

During the 14-day observation period, no mortality or overt clinical signs of toxicity were recorded in any of the treated animals, indicating the hydrogel's favorable biocompatibility [141].

### 4.10.1 Weight and Clinical Observations

As Body weight is an indicator of systemic health so it is assessed at specified intervals (Days 1, 7, and 14). Weight gain was similar in both groups (control and treated) over the study period with no statistically significant differences calculated ($p$>0.05, unpaired t-test) (as shown as Table 4.4).

General behavior monitoring animals demonstrated normal locomotor activity, grooming behavior, food, and water intake, and their general appearance via subjective assessment was consistent in all animals during the study. There were still no observations of salivation, piloerection, tremors, convulsions, or lethargy as the study progressed which further confirmed that there were no observable treatment-related neurobehavioral or metabolic consequences.

### 4.10.2 Hematological and Biochemical Evaluation

The findings of the hematological analysis showed no differences in key indicators, including hemoglobin, total and differential leukocytes, and platelets, between the experimental and control groups ($p$>0.05), as seen in Table 5. Likewise, biochemical indicators of liver and kidney function, including ALT, AST, ALP; increased creatinine and urea; were all within the reference range for both experimental and control groups and did not show any statistically significant variations ($p$>0.05). Blood glucose also showed no impact, indicating the absence of hydrogel-induced metabolic disturbances as shown as Table 4.5.

### 4.10.3 Histopathological Analysis

Microscopic examination of the following essential organs; liver, kidneys, heart, spleen, stomach, and intestines showed their tissue morphology was preserved. There was no evidence of inflammation, necrosis, cellular degeneration, or other pathological lesions in either group. Histological images of representative tissues are illustrated in Figure 4.12, indicating that hydrogel administration did not result in organ toxicity or structural damage. The hydrogel formulation was well tolerated by all test groups, and the lack of mortality, clinical abnormalities, absence of abnormal hematology or biochemistry finding and histopathological lesions illustrated that systemic toxicity is not apparent following oral hydrogel administration. This signifies safety of the hydrogel formulation; therefore in vivo efficacy and pharmacokinetic trials can be undertaken.

TABLE 4.4: Summary of Clinical Observations in Acute Oral Toxicity Study.

| **Parameter** | **Control Group (Mean ± SD)** | **Treated Group (Mean ± SD)** | **Interpretation** |
|---|---|---|---|
| **Body Weight (g)** | Day 1: 25.5 ± 1.2 | Day 1: 25.2 ± 1.1 | No significant difference |
| | Day 7: 26.5 ± 1.0 | Day 7: 26.0 ± 1.2 | ($p > 0.05$) |
| | Day 14: 27.8 ± 1.3 | Day 14: 27.5 ± 1.2 | |
| **Food Intake (g/day)** | Day 1: 4.5 ± 0.2 | Day 1: 4.6 ± 0.3 | Normal intake maintained |
| | Day 7: 5.3 ± 0.3 | Day 7: 5.5 ± 0.2 | |
| | Day 14: 6.0 ± 0.3 | Day 14: 5.9 ± 0.2 | |
| **Water Intake (mL/day)** | Day 1: 5.2 ± 0.4 | Day 1: 5.3 ± 0.2 | Normal intake maintained |
| | Day 7: 5.7 ± 0.3 | Day 7: 5.8 ± 0.4 | |
| | Day 14: 6.5 ± 0.6 | Day 14: 6.4 ± 0.3 | |
| **Locomotor Activity** | Normal throughout | Normal throughout | No observable abnormalities |
| **Grooming Behavior** | Normal throughout | Normal throughout | No observable abnormalities |

continued on next page

**Table 4.4 continued from previous page**

| Parameter | Control Group (Mean ± SD) | Treated Group (Mean ± SD) | Interpretation |
|---|---|---|---|
| **Salivation** | Absent | Absent | No adverse effects |
| **Piloerection** | Absent | Absent | No adverse effects |
| **Convulsions / Tremors** | Absent | Absent | No adverse effects |
| **Lethargy** | Absent | Absent | No adverse effects |

TABLE 4.5: Hematological and Biochemical Parameters in Acute Oral Toxicity Study.

| Parameter | Control Group (Mean ± SD) | Treated Group (Mean ± SD) | p-value | Interpretation |
|---|---|---|---|---|
| **Hemoglobin (g/dL)** | 13.6 ± 0.5 | 13.8 ± 0.4 | >0.05 | No significant difference |
| **WBC ($10^3/mm^3$)** | 7.3 ± 0.4 | 7.1 ± 0.5 | >0.05 | Within normal limits |
| **Platelets ($10^3/mm^3$)** | 248 ± 11 | 252 ± 12 | >0.05 | No treatment-related alterations |
| **ALT (U/L)** | 33.0 ± 2.5 | 32.5 ± 2.2 | >0.05 | Hepatic function unaffected |
| **AST (U/L)** | 28.8 ± 1.7 | 28.4 ± 1.9 | >0.05 | Hepatic function unaffected |
| **ALP (U/L)** | 73.5 ± 3.2 | 72.8 ± 3.0 | >0.05 | Hepatic function unaffected |
| **Creatinine (mg/dL)** | 0.82 ± 0.04 | 0.80 ± 0.05 | >0.05 | Renal function unaffected |
| **Urea (mg/dL)** | 21.9 ± 1.4 | 22.3 ± 1.2 | >0.05 | Renal function unaffected |
| **Glucose (mg/dL)** | 91.8 ± 3.3 | 92.5 ± 3.6 | >0.05 | No metabolic disturbances observed |

**Note:** Results expressed as mean ± SD; n = 5 animals per group.

Statistical comparison performed using unpaired t-test.

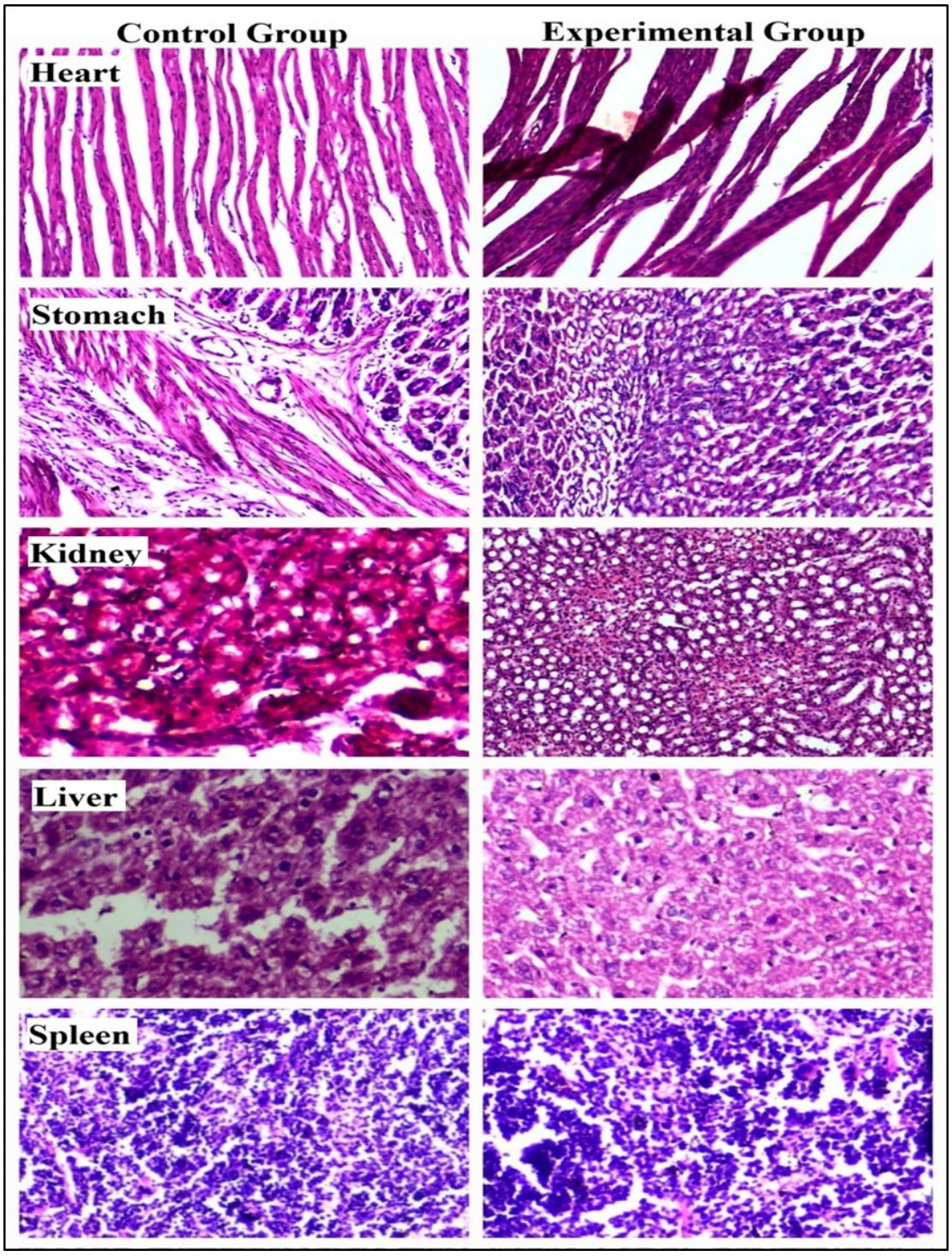


FIGURE 4.12: Histopathological evaluation of vital organs from control and treated groups. All organs exhibited preserved tissue architecture with no signs of cellular damage, inflammation, or structural abnormalities (H&E staining, 40× magnification).

# Chapter 5

# Conclusion and Future Recommendations

## 5.1 Conclusion

The developed rosuvastatin-loaded pH-sensitive hydrogel system was superior in exhibiting controlled and targeted drug delivery. The swelling behavior exhibited an excellent pH-sensitive swelling phenomenon, with increased swelling at pH 7.4 under acidic conditions, verifying the pH sensitivity of the hydrogel based on the ionization nature of the added polymers and monomer (acrylic acid). In vitro release profiles also confirmed such effects, with low drug release under acidic environment (pH 1.2), and thus avoiding gastric release, in accordance with sustained, augmented release at pH 7.4, reflecting intestinal drug delivery preferability. DSC and TGA analysis validated the thermal stability of the hydrogel network and effective drug encapsulation with no phase change or degradation of rosuvastatin. SEM micrographs showed porous and networked surface morphology, which allows for effective entrapment of the drug and diffusion. FTIR spectra revealed no characteristic chemical interaction between drug and excipients, maintaining compatibility and integrity of the drug. In addition, solubility tests showed that there was a significant increase in rosuvastatin solubility when encapsulated in the

hydrogel matrix, especially at pH 7.4, consistent with its site of activity. The enhanced solubility along with the sustained release pattern should cause increased oral bioavailability of rosuvastatin by avoiding solubility-limited absorption in the stomach leading to facilitation of more efficient absorption in the intestines. The results of biocompatibility study are supportive of the wolves that the developed rosuvastatin hydrogel can be delivered orally without any adverse effects and can be subsequently investigated with respect to pharmacodynamics and pharmacokinetics. In conclusion, the findings validate the hydrogel as a viable oral delivery system for the enhancement of the therapeutic efficacy of weakly soluble and pH-sensitive drugs such as rosuvastatin.

## 5.2 Future Recommendations

With the promising results of the current study, pH-responsive rosuvastatin-loaded hydrogels show significant potential for improved solubility in drug delivery and controlled release in a site-specific manner. Future studies should utilize the optimized formulation in a scaled-up form (in larger batches) in conjunction with conduct in vivo pharmacokinetic and pharmacodynamic studies to deliver and demonstrate bioavailability and efficacy in animal models. In addition, mucoadhesive studies, and possibly studying gastrointestinal transit behavior can be performed to confirm their site-specific release of drug delivery. Future iterations of this hydrogel system could also incorporate more efficient delivery strategies, including conjugation of ligands to facilitate receptor-mediated uptake. It is also recommended that long-term stability studies following ICH (International Council for Harmonization) guidelines, and chronic toxicity evaluations be performed to provide support for eventual clinical translation. Since the hydrogels were designed for site-specific delivery of rosuvastatin, the hydrogel platform may be explored as a means of co-delivery of synergistic agents, or other poorly soluble forms of statins to broaden its potential for cardiovascular therapies and lipid lowering therapeutics.

# Bibliography

[1] B. Şahin and G. İlgün, "Risk factors of deaths related to cardiovascular diseases in world health organization (who) member countries," *Health & Social Care in the Community*, vol. 30, no. 1, pp. 73–80, 2022.

[2] D. Zhao, "Epidemiological features of cardiovascular disease in asia," *JACC: Asia*, vol. 1, no. 1, pp. 1–13, 2021.

[3] C. R. Wei *et al.*, "Comparison of the efficacy of atorvastatin with rosuvastatin in preventing cardiovascular events among patients with cardiovascular disease: a meta-analysis," *Cureus*, vol. 15, no. 12, 2023.

[4] V. Barrios and C. Escobar, "Fixed-dose combination of rosuvastatin and ezetimibe: treating hypercholesteremia according to cardiovascular risk," *Expert Review of Clinical Pharmacology*, vol. 14, no. 7, pp. 793–806, 2021.

[5] C. M. Bowman *et al.*, "Improving the translation of organic anion transporting polypeptide substrates using hek293 cell data in the presence and absence of human plasma via physiologically based pharmacokinetic modeling," *Drug Metabolism and Disposition*, vol. 49, no. 7, pp. 530–539, 2021.

[6] H. Shoukat *et al.*, "Enhancing solubility and oral bioavailability of rosuvastatin through interpenetrating polymer network (ipn) nanogels: Fabrication, characterization, and in-vivo efficacy assessment," *Journal of Drug Delivery Science and Technology*, vol. 98, p. 105866, 2024.

[7] R. González *et al.*, "Design, development, and characterization of amorphous rosuvastatin calcium tablets," *PLoS One*, vol. 17, no. 3, p. e0265263, 2022.

[8] R. Devarapalli *et al.*, "Investigation of poor solubility of a salt-cocrystal hydrate: A case study of the common-ion effect in betrixaban, an anticoagulant drug," *Molecular Pharmaceutics*, vol. 18, no. 3, pp. 1138–1149, 2021.

[9] K. U. Khan *et al.*, "Overview of nanoparticulate strategies for solubility enhancement of poorly soluble drugs," *Life Sciences*, vol. 291, p. 120301, 2022.

[10] L. Strilchuk *et al.*, "An overview of rosuvastatin/ezetimibe association for the treatment of hypercholesterolemia and mixed dyslipidemia," *Expert Opinion on Pharmacotherapy*, vol. 21, no. 5, pp. 531–539, 2020.

[11] P. Matricardi *et al.*, "Interpenetrating polymer networks polysaccharide hydrogels for drug delivery and tissue engineering," *Advanced Drug Delivery Reviews*, vol. 65, no. 9, pp. 1172–1187, 2013.

[12] B. Ye, R. Xiang, and F. Luo, "Hydrogel-based drug delivery systems for diabetes bone defects," *Chemical Engineering Journal*, p. 154436, 2024.

[13] C. I. Idumah *et al.*, "Recent advances in polymeric hydrogel nanoarchitectures for drug delivery applications," *International Journal of Polymeric Materials and Polymeric Biomaterials*, vol. 73, no. 1, pp. 1–32, 2024.

[14] J. Weng, H. H. Tong, and S. F. Chow, "In vitro release study of the polymeric drug nanoparticles: development and validation of a novel method," *Pharmaceutics*, vol. 12, no. 8, p. 732, 2020.

[15] N. H. Thang, T. B. Chien, and D. X. Cuong, "Polymer-based hydrogels applied in drug delivery: An overview," *Gels*, vol. 9, no. 7, p. 523, 2023.

[16] M. Vázquez-González and I. Willner, "Stimuli-responsive biomolecule-based hydrogels and their applications," *Angewandte Chemie International Edition*, vol. 59, no. 36, pp. 15342–15377, 2020.

[17] S. Xian and M. J. Webber, "Temperature-responsive supramolecular hydrogels," *Journal of Materials Chemistry B*, vol. 8, no. 40, pp. 9197–9211, 2020.

[18] M. Sobczak, "Enzyme-responsive hydrogels as potential drug delivery systems—state of knowledge and future prospects," *International Journal of Molecular Sciences*, vol. 23, no. 8, p. 4421, 2022.

[19] Y. He *et al.*, "Magnetic hydrogel-based flexible actuators: A comprehensive review on design, properties, and applications," *Chemical Engineering Journal*, vol. 462, p. 142193, 2023.

[20] Y. Xing, B. Zeng, and W. Yang, "Light responsive hydrogels for controlled drug delivery," *Frontiers in Bioengineering and Biotechnology*, vol. 10, p. 1075670, 2022.

[21] H. Ding *et al.*, "Preparation and application of ph-responsive drug delivery systems," *Journal of Controlled Release*, vol. 348, pp. 206–238, 2022.

[22] B. Liu and K. Chen, "Advances in hydrogel-based drug delivery systems," *Gels*, vol. 10, no. 4, p. 262, 2024.

[23] S. Zhuo *et al.*, "ph-sensitive biomaterials for drug delivery," *Molecules*, vol. 25, no. 23, p. 5649, 2020.

[24] J. Singh and P. Nayak, "ph-responsive polymers for drug delivery: trends and opportunities," *Journal of Polymer Science*, vol. 61, no. 22, pp. 2828–2850, 2023.

[25] S. S. Gomte *et al.*, "Exploring the potential of ph-sensitive polymers in targeted drug delivery," *Journal of Biomaterials Science, Polymer Edition*, vol. 35, no. 2, pp. 228–268, 2024.

[26] T. Mahmood *et al.*, "Preparation, in vitro characterization, and evaluation of polymeric ph-responsive hydrogels for controlled drug release," *ACS Omega*, vol. 9, no. 9, pp. 10498–10516, 2024.

[27] Y. Mu *et al.*, "Advances in ph-responsive drug delivery systems," *OpenNano*, vol. 5, p. 100031, 2021.

[28] A. Ghaffar *et al.*, "ph-sensitive drug delivery systems," in *Metal Nanoparticles for Drug Delivery and Diagnostic Applications*, pp. 259–278, Elsevier, 2020.

[29] X. Tong *et al.*, "Recent advances in natural polymer-based drug delivery systems," *Reactive and Functional Polymers*, vol. 148, p. 104501, 2020.

[30] W. Cui and L. Xiang, *Natural Polymers for Biomedical Applications*. John Wiley & Sons, 2024.

[31] J. Yang *et al.*, "Constructions and properties of physically cross-linked hydrogels based on natural polymers," *Polymer Reviews*, vol. 63, no. 3, pp. 574–612, 2023.

[32] Z. Terzopoulou *et al.*, "Biocompatible synthetic polymers for tissue engineering purposes," *Biomacromolecules*, vol. 23, no. 5, pp. 1841–1863, 2022.

[33] A. Sharma *et al.*, "Understanding the journey of biopolymeric nanoformulations for oral drug delivery: Conventional to advanced treatment approaches," *European Polymer Journal*, p. 113338, 2024.

[34] M. Lapointe and B. Barbeau, "Understanding the roles and characterizing the intrinsic properties of synthetic vs. natural polymers to improve clarification through interparticle bridging: A review," *Separation and Purification Technology*, vol. 231, p. 115893, 2020.

[35] F. Khan *et al.*, "Synthesis, classification and properties of hydrogels: Their applications in drug delivery and agriculture," *Journal of Materials Chemistry B*, vol. 10, no. 2, pp. 170–203, 2022.

[36] A. Mtibe *et al.*, "Synthetic biopolymers and their composites: Advantages and limitations—an overview," *Macromolecular Rapid Communications*, vol. 42, no. 15, p. 2100130, 2021.

[37] G. Satchanska, S. Davidova, and P. D. Petrov, "Natural and synthetic polymers for biomedical and environmental applications," *Polymers*, vol. 16, no. 8, p. 1159, 2024.

[38] D. M. Yoon and J. P. Fisher, "Natural and synthetic polymeric scaffolds," *Biomedical Materials*, pp. 257–283, 2021.

[39] M. Mohammed *et al.*, "Comprehensive insights on mechanical attributes of natural-synthetic fibres in polymer composites," *Journal of Materials Research and Technology*, vol. 25, pp. 4960–4988, 2023.

[40] S. Begum, S. Fawzia, and M. Hashmi, "Polymer matrix composite with natural and synthetic fibres," *Advances in Materials and Processing Technologies*, vol. 6, no. 3, pp. 547–564, 2020.

[41] F. Andrade *et al.*, "Stimuli-responsive hydrogels for cancer treatment: The role of ph, light, ionic strength and magnetic field," *Cancers*, vol. 13, no. 5, p. 1164, 2021.

[42] Y. Hu *et al.*, "A double-layer hydrogel based on alginate-carboxymethyl cellulose and synthetic polymer as sustained drug delivery system," *Scientific Reports*, vol. 11, no. 1, p. 9142, 2021.

[43] P. Bramhe *et al.*, "Polymer blends innovation: Advancement in novel drug delivery," *International Journal of Polymeric Materials and Polymeric Biomaterials*, vol. 74, no. 10, pp. 957–974, 2025.

[44] M. A. Grimaudo, A. Concheiro, and C. Alvarez-Lorenzo, "Nanogels for regenerative medicine," *Journal of Controlled Release*, vol. 313, pp. 148–160, 2019.

[45] A. Hendi *et al.*, "Healthcare applications of ph-sensitive hydrogel-based devices: a review," *International Journal of Nanomedicine*, pp. 3887–3901, 2020.

[46] L. Li *et al.*, "Progress on preparation of ph/temperature-sensitive intelligent hydrogels and applications in target transport and controlled release of drugs," *International Journal of Polymer Science*, vol. 2021, no. 1, p. 1340538, 2021.

[47] G. Sworn, "Xanthan gum," in *Handbook of Hydrocolloids*, pp. 833–853, Elsevier, 2021.

[48] I. F. Furtado *et al.*, "Xanthan gum: applications, challenges, and advantages of this asset of biotechnological origin," *Biotechnology Research and Innovation Journal*, vol. 6, no. 1, pp. 0–0, 2022.

[49] S. Chaturvedi *et al.*, "A review on properties and applications of xanthan gum," in *Microbial Polymers: Applications and Ecological Perspectives*, pp. 87–107, 2021.

[50] I. M. Bhat *et al.*, "Advances in xanthan gum production, modifications and its applications," *Biocatalysis and Agricultural Biotechnology*, vol. 42, p. 102328, 2022.

[51] A. Mehrabi *et al.*, "Evaluation of inherent properties of the carboxymethyl cellulose (cmc) for potential application in tissue engineering focusing on bone regeneration," *Polymers for Advanced Technologies*, vol. 35, no. 1, p. e6258, 2024.

[52] S. Li *et al.*, "Fabrication and characterization of a novel semi-interpenetrating network hydrogel based on sodium carboxymethyl cellulose and poly (methacrylic acid) for oral insulin delivery," *Journal of Biomaterials Applications*, vol. 35, no. 1, pp. 3–14, 2020.

[53] I. Aranaz *et al.*, "Chitosan: An overview of its properties and applications," *Polymers*, vol. 13, no. 19, p. 3256, 2021.

[54] F. Hong *et al.*, "Chitosan-based hydrogels: From preparation to applications, a review," *Food Chemistry: X*, vol. 21, p. 101095, 2024.

[55] A. Saleem *et al.*, "Highly responsive chitosan-co-poly (maa) nanomatrices through cross-linking polymerization for solubility improvement," *Gels*, vol. 8, no. 3, p. 196, 2022.

[56] M. Wang *et al.*, "Preparation of ph-sensitive carboxymethyl cellulose/chitosan/alginate hydrogel beads with reticulated shell structure to deliver *Bacillus subtilis* natto," *International Journal of Biological Macromolecules*, vol. 192, pp. 684–691, 2021.

[57] N. S. Malik *et al.*, "Chitosan/xanthan gum based hydrogels as potential carrier for an antiviral drug: Fabrication, characterization, and safety evaluation," *Frontiers in Chemistry*, vol. 8, p. 50, 2020.

[58] W. Wang *et al.*, "A ph-responsive carboxymethyl cellulose/chitosan hydrogel for adsorption and desorption of anionic and cationic dyes," *Cellulose*, vol. 28, pp. 897–909, 2021.

[59] L. Yu *et al.*, "Fabrication of a poly (gallic acid) nanoparticle-reinforced chitosan/xanthan gum hydrogel for treating diabetic oral ulcers," *Colloids and Surfaces A: Physicochemical and Engineering Aspects*, p. 137247, 2025.

[60] R. Kanukula *et al.*, "Pharmacokinetics of rosuvastatin: a systematic review of randomised controlled trials in healthy adults," *Clinical Pharmacokinetics*, vol. 60, pp. 165–175, 2021.

[61] S. M. El-Masry *et al.*, "Bio-friendly oleic acid-based ufasomal topical gel of rosuvastatin for diabetic wound healing: In-vitro, ex-vivo, and in-vivo evaluation," *Journal of Drug Delivery Science and Technology*, vol. 97, p. 105789, 2024.

[62] T. M. Shehata, B. Aldhubiab, and H. S. Elsewedy, "Virgin coconut oil-based nanostructured lipid carrier improves the hypolipidemic effect of rosuvastatin," *International Journal of Nanomedicine*, pp. 7945–7961, 2024.

[63] S. Younas *et al.*, "Synthesis and evaluation of transdermal rosuvastatin-loaded ultradeformable vesicles: Restoring the serum lipid profile in poloxamer 407-caused hyperlipidemia," *Journal of Drug Delivery Science and Technology*, vol. 102, p. 106330, 2024.

[64] S. F. Badshah *et al.*, "Structural and in-vitro characterization of highly swellable -cyclodextrin polymeric nanogels fabricated by free radical polymerization for solubility enhancement of rosuvastatin," *Particulate Science and Technology*, vol. 41, no. 8, pp. 1131–1145, 2023.

[65] I. M. Adel *et al.*, "Polymeric nanocomposite hydrogel scaffold for jawbone regeneration: The role of rosuvastatin calcium-loaded silica nanoparticles," *International Journal of Pharmaceutics: X*, vol. 6, p. 100213, 2023.

[66] H. F. Salem *et al.*, "Rosuvastatin calcium-based novel nanocubic vesicles capped with silver nanoparticles-loaded hydrogel for wound healing management: optimization employing box–behnken design: in vitro and in vivo assessment," *Journal of Liposome Research*, vol. 32, no. 1, pp. 45–61, 2022.

[67] T. A. Ahmed, "Study the pharmacokinetics, pharmacodynamics and hepatoprotective activity of rosuvastatin from drug loaded lyophilized orodispersible tablets containing transfersomes nanoparticles," *Journal of Drug Delivery Science and Technology*, vol. 63, p. 102489, 2021.

[68] N. M. Sweed *et al.*, "Response surface optimization of self nano-emulsifying drug delivery system of rosuvastatin calcium for hepatocellular carcinoma," *Journal of Pharmaceutical Investigation*, vol. 51, pp. 85–101, 2021.

[69] I. Elsayed *et al.*, "Response surface optimization of biocompatible elastic nanovesicles loaded with rosuvastatin calcium: enhanced bioavailability and anticancer efficacy," *Drug Delivery and Translational Research*, vol. 10, pp. 1459–1475, 2020.

[70] K. M. Hosny, W. Y. Rizg, and R. A. Khallaf, "Preparation and optimization of in situ gel loaded with rosuvastatin-ellagic acid nanotransfersomes to enhance the anti-proliferative activity," *Pharmaceutics*, vol. 12, no. 3, p. 263, 2020.

[71] R. M. Sarfraz *et al.*, "Development and evaluation of rosuvastatin calcium based microparticles for solubility enhancement: an in vitro study," *Advances in Polymer Technology*, vol. 36, no. 4, pp. 433–441, 2017.

[72] J. Patel, S. Maiti, and N. H. N. Moorthy, "Repaglinide-laden hydrogel particles of xanthan gum derivatives for the management of diabetes," *Carbohydrate Polymers*, vol. 287, p. 119354, 2022.

[73] M. I. Asad *et al.*, "Development and in vitro/in vivo evaluation of ph-sensitive polymeric nanoparticles loaded hydrogel for the management of psoriasis," *Nanomaterials*, vol. 11, no. 12, p. 3433, 2021.

[74] N. Richbourg *et al.*, "Precise control of synthetic hydrogel network structure via linear, independent synthesis-swelling relationships," *Science Advances*, vol. 7, no. 7, p. eabe3245, 2021.

[75] M. U. A. Khan *et al.*, "Antibacterial and hemocompatible ph-responsive hydrogel for skin wound healing application: In vitro drug release," *Polymers*, vol. 13, no. 21, p. 3703, 2021.

[76] P. Wang, Z.-g. Luo, and Z.-g. Xiao, "Preparation, physicochemical characterization and in vitro release behavior of resveratrol-loaded oxidized gellan gum/resistant starch hydrogel beads," *Carbohydrate Polymers*, vol. 260, p. 117794, 2021.

[77] S. Magalhães, B. J. Goodfellow, and A. Nunes, "Ftir spectroscopy in biomedical research: How to get the most out of its potential," *Applied Spectroscopy Reviews*, vol. 56, no. 8-10, pp. 869–907, 2021.

[78] F. N. Al-Heibshy *et al.*, "Physicochemical characterization and pharmacokinetic evaluation of rosuvastatin calcium incorporated solid lipid nanoparticles," *International Journal of Pharmaceutics*, vol. 578, p. 119106, 2020.

[79] M. Iijima, T. Hatakeyama, and H. Hatakeyama, "Dsc and tma studies of polysaccharide physical hydrogels," *Analytical Sciences*, vol. 37, no. 1, pp. 211–219, 2021.

[80] Z. Ul Hassan Shah *et al.*, "Development of antihyperlipidemic drug loaded -cd-based microparticulate carrier systems: tuning and optimization," *Polymer-Plastics Technology and Materials*, vol. 63, no. 11, pp. 1438–1463, 2024.

[81] S. Naeem *et al.*, "Fabrication of ph responsive hydrogel blends of chondroitin sulfate/pluronic f-127 for the controlled release of ketorolac: Its characterization and acute oral toxicity study," *Drug Development and Industrial Pharmacy*, vol. 48, no. 11, pp. 611–622, 2022.

[82] B. Kaczmarek, K. Nadolna, and A. Owczarek, "The physical and chemical properties of hydrogels based on natural polymers," in *Hydrogels Based on Natural Polymers*, pp. 151–172, 2020.

[83] C. López-Manzanara Pérez *et al.*, "Development of chitosan/sodium carboxymethylcellulose complexes to improve the simvastatin release rate: Polymer/polymer and drug/polymer interactions' effects on kinetic models," *Polymers*, vol. 15, no. 20, p. 4184, 2023.

[84] M.-Y. Wu *et al.*, "Effects of adding chitosan on drug entrapment efficiency and release duration for paclitaxel-loaded hydroxyapatite—gelatin composite microspheres," *Pharmaceutics*, vol. 15, no. 8, p. 2025, 2023.

[85] N. Batool *et al.*, "Formulation and evaluation of interpenetrating polymeric network for controlled drug delivery," *Drug Development and Industrial Pharmacy*, vol. 47, no. 6, pp. 931–946, 2021.

[86] N. S. Malik *et al.*, "Corrigendum: Chitosan/xanthan gum based hydrogels as potential carrier for an antiviral drug: Fabrication, characterization, and safety evaluation," *Frontiers in Chemistry*, vol. 10, p. 1083154, 2023.

[87] L. Li *et al.*, "A ph-sensitive and sustained-release oral drug delivery system: the synthesis, characterization, adsorption and release of the xanthan gum-graft-poly (acrylic acid)/go–dcfp composite hydrogel," *RSC Advances*, vol. 11, no. 42, pp. 26229–26240, 2021.

[88] S. Hossieni-Aghdam, H. Motsadizadeh, and H. Farhadnejad, "Facile fabrication and characterization of a novel oral ph-sensitive drug delivery system based on cmc hydrogel and hnt-at nanohybrid," *International Journal of Biological Macromolecules*, vol. 113, pp. 2436–2449, 2018.

[89] I. P. Merlusca *et al.*, "Characterization of neomycin-loaded xanthan-chitosan hydrogels for topical applications," *Cellulose Chemistry and Technology*, vol. 53, no. 7–8, pp. 709–719, 2019.

[90] W. Zhang *et al.*, "Factors affecting the properties of superabsorbent polymer hydrogels and methods to improve their performance: a review," *Journal of Materials Science*, vol. 56, pp. 16223–16242, 2021.

[91] I. M. Adel *et al.*, "Gellan gum-based bi-polymeric hydrogel scaffolds loaded with rosuvastatin calcium: A useful tool for tendon tissue regeneration," *European Journal of Pharmaceutical Sciences*, vol. 192, p. 106659, 2024.

[92] J. Yang *et al.*, "Advanced applications of chitosan-based hydrogels: From biosensors to intelligent food packaging system," *Trends in Food Science & Technology*, vol. 110, pp. 822–832, 2021.

[93] K. Mukherjee *et al.*, "Xanthan gum and its composite-based hydrogels," in *Polysaccharide Hydrogels for Drug Delivery and Regenerative Medicine*, pp. 89–108, Elsevier, 2024.

[94] A. Sorokin *et al.*, "A new approach to increasing the equilibrium swelling ratio of the composite superabsorbents based on carboxymethyl cellulose sodium salt," *Cellulose*, vol. 29, no. 1, pp. 159–173, 2022.

[95] M. R. Jozaghkar, A. Sepehrian Azar, and F. Ziaee, "Preparation, characterization, and swelling study of n, n'-dimethylacrylamide/acrylic acid amphiphilic hydrogels in different conditions," *Polymer Bulletin*, vol. 79, no. 7, pp. 5183–5195, 2022.

[96] Z. Wei *et al.*, "The thermal stability mechanism of mba-crosslinked ppgs: Insights from macroscopic phenomena to chemical reactions," *Polymer*, vol. 309, p. 127460, 2024.

[97] R. M. Sarfraz *et al.*, "Development, in vitro and in vivo evaluation of ph responsive -cd-comethacrylic acid-crosslinked polymeric microparticulate system for solubility enhancement of rosuvastatin calcium," *Polymer-Plastics Technology and Engineering*, vol. 57, no. 12, pp. 1175–1187, 2018.

[98] Y. Li *et al.*, "Preparation of carboxymethylcellulose/zno/chitosan composite hydrogel microbeads and its drug release behaviour," *International Journal of Biological Macromolecules*, vol. 247, p. 125716, 2023.

[99] L. Djekic and A. Ćirić, "Micro-and nanoscale drug delivery systems based on xanthan gum hydrogels," in *Micro-and Nanoengineered Gum-Based Biomaterials for Drug Delivery and Biomedical Applications*, pp. 35–76, Elsevier, 2022.

[100] A. Khan *et al.*, "Sustained release delivery of favipiravir through statistically optimized, chemically cross-linked, ph-sensitive, swellable hydrogel," *BMC Pharmacology and Toxicology*, vol. 25, no. 1, p. 31, 2024.

[101] J. Safari, A. Bapolisi, and R. Krause, "Development of ph-sensitive chitosan-g-poly (acrylamide-co-acrylic acid) hydrogel for controlled drug delivery of tenofovir disoproxil fumarate," *Polymers*, vol. 13, no. 20, p. 3571, 2021.

[102] M. Cheng *et al.*, "Design of carboxymethyl chitosan-reinforced ph-responsive hydrogels for on-demand release of carvacrol and simulation of release kinetics," *Food Chemistry*, vol. 405, p. 134856, 2023.

[103] Y. Tkachenko and P. Niedzielski, "Ftir as a method for qualitative assessment of solid samples in geochemical research: a review," *Molecules*, vol. 27, no. 24, p. 8846, 2022.

[104] P. Pawar, V. Sinha, and A. Yadav, "Compatibility study and solid dose formulation of rosuvastatin calcium," *Journal of Modern Pharmacology and Pathology*, 2024.

[105] M. Gharibshahian *et al.*, "Fabrication of rosuvastatin-incorporated polycaprolactone-gelatin scaffold for bone repair: a preliminary in vitro study," *Cell Journal (Yakhteh)*, vol. 26, no. 1, p. 70, 2024.

[106] N. Nordin *et al.*, "Efficient encapsulation of a model drug in chitosan cathodic electrodeposition: Preliminary analysis using ftir, uv–vis, and nmr spectroscopy," *Carbohydrate Polymers*, vol. 348, p. 122830, 2025.

[107] W. Meng *et al.*, "Pickering emulsions with chitosan and macroalgal polyphenols stabilized by layer-by-layer electrostatic deposition," *Carbohydrate Polymers*, vol. 300, p. 120256, 2023.

[108] M. Arulmoorthy *et al.*, "Biosynthesis and characterization of chitosan based hydrogel: A potential in vitro wound healing agent," *Materials Today: Proceedings*, vol. 48, pp. 263–275, 2022.

[109] Y. Sheng *et al.*, "Dual-drug delivery system based on the hydrogels of alginate and sodium carboxymethyl cellulose for colorectal cancer treatment," *Carbohydrate Polymers*, vol. 269, p. 118325, 2021.

[110] C. Cui *et al.*, "Curdlan/sodium carboxymethylcellulose composite adsorbents: A biodegradable solution for organic dye removal from water," *Carbohydrate Polymers*, vol. 328, p. 121737, 2024.

[111] S. Tan *et al.*, "Storage stability and in vitro release characteristics of black rice anthocyanins microencapsulated by pectin and sodium carboxymethyl cellulose," *LWT*, vol. 207, p. 116654, 2024.

[112] S. Huang *et al.*, "Development and characterization of biodegradable antibacterial hydrogels of xanthan gum for controlled ciprofloxacin release," *International Journal of Biological Macromolecules*, vol. 309, p. 142637, 2025.

[113] T. Nnyigide, O. Nnyigide, and K. Hyun, "Rheological characterization of a novel synergistic bovine serum albumin–xanthan gum composite hydrogel," *Korea-Australia Rheology Journal*, pp. 1–23, 2025.

[114] H. Hayrabolulu *et al.*, "Radiation synthesis and characterization of xanthan gum hydrogels," *Radiation Physics and Chemistry*, vol. 188, p. 109613, 2021.

[115] Z. Chen *et al.*, "Structure and properties of cellulose strengthened poly (acrylic acid) hydrogels," *Macromolecular Materials and Engineering*, vol. 309, no. 9, p. 2300454, 2024.

[116] G. Bardajee, R. Ghadimkhani, and F. Jafarpour, "A biocompatible double network hydrogel based on poly (acrylic acid) grafted onto sodium alginate

for doxorubicin hydrochloride anticancer drug release," *International Journal of Biological Macromolecules*, vol. 260, p. 128871, 2024.

[117] H. Tuan *et al.*, "Effect of n, n -methylenebisacrylamide on properties of porous semi-ipn hydrogels from acrylamide, maleic acid, and its use for urea absorption," *Canadian Journal of Chemistry*, vol. 103, no. 2, pp. 46–59, 2024.

[118] P. Meena, P. Singh, and S. Warkar, "Development and assessment of carboxymethyl tamarind kernel gum-based ph-responsive hydrogel for release of diclofenac sodium," *European Polymer Journal*, vol. 197, p. 112340, 2023.

[119] N. S. El-Salamouni *et al.*, "Rosuvastatin/calcium carbonate co-precipitated nanoparticles: A novel synergistic approach enhancing local bone regeneration in osteoporotic rat model," *International Journal of Pharmaceutics*, vol. 668, p. 124977, 2025.

[120] M. R. Ghahfarokhi, G. Dini, and B. Movahedi, "Fabrication of chitosan-coated mesoporous silica nanoparticles bearing rosuvastatin as a drug delivery system," *Current Drug Delivery*, vol. 19, no. 1, pp. 64–73, 2022.

[121] P. Zhou *et al.*, "Construction of chitosan/ag nanocomposite sponges and their properties," *International Journal of Biological Macromolecules*, vol. 192, pp. 272–277, 2021.

[122] X. Zhu *et al.*, "Ion-responsive chitosan hydrogel actuator inspired by carrotwood seed pod," *Carbohydrate Polymers*, vol. 276, p. 118759, 2022.

[123] M. Fan *et al.*, "Synthesis, characterization, and photocatalytic activity of a carboxymethyl cellulose sodium-based hybrid material for efficient degradation of hexavalent chromium," *International Journal of Biological Macromolecules*, vol. 306, p. 141536, 2025.

[124] Z. Wu *et al.*, "Synthesis, characterization, and methylene blue adsorption of multiple-responsive hydrogels loaded with huangshui polysaccharides, polyvinyl alcohol, and sodium carboxyl methyl cellulose," *International Journal of Biological Macromolecules*, vol. 216, pp. 157–171, 2022.

[125] K. Chen *et al.*, "Preparation and characterization of polyvinyl alcohol/-sodium alginate/carboxymethyl cellulose composite hydrogels with oriented structure," *Soft Materials*, vol. 20, no. 1, pp. 99–108, 2022.

[126] I. Saha *et al.*, "Topical effect of polyherbal flowers extract on xanthan gum hydrogel patch—induced wound healing activity in human cell lines and male balb/c mice," *Biomedical Materials*, vol. 18, no. 3, p. 035016, 2023.

[127] W. M. Seleka and E. Makhado, "Synthesis and characterization xanthan gum/acrylic acid/acrylamide modified with graphene oxide hydrogel nanocomposite for removal of methylene blue from aqueous solution," *International Journal of Biological Macromolecules*, p. 141015, 2025.

[128] A. Ullah *et al.*, "Development and evaluation of bioinspired ph-responsive sericin–chitosan-based hydrogel for controlled colonic delivery of petase: Harnessing petase-triggered degradation of microplastics," *International Journal of Biological Macromolecules*, vol. 242, p. 124698, 2023.

[129] R. Ye *et al.*, "Synthesis, characterization, properties, and biomedical application of chitosan-based hydrogels," *Polymers*, vol. 15, no. 11, p. 2482, 2023.

[130] M. Kang *et al.*, "Characterization of xanthan gum-based hydrogel with $fe^{3+}$ ions coordination and its reversible sol-gel conversion," *Carbohydrate Polymers*, vol. 203, pp. 139–147, 2019.

[131] N. F. A.-Z. Tuan Mohamood, A. H. Abdul Halim, and N. Zainuddin, "Carboxymethyl cellulose hydrogel from biomass waste of oil palm empty fruit bunch using calcium chloride as crosslinking agent," *Polymers*, vol. 13, no. 23, p. 4056, 2021.

[132] F. Ghasemvand *et al.*, "Chitosan, polyethylene oxide/polycaprolactone electrospun core/shell nanofibrous mat containing rosuvastatin as a novel drug delivery system for enhancing human mesenchymal stem cell osteogenesis," *Frontiers in Molecular Biosciences*, vol. 10, p. 1220357, 2023.

[133] H. Shoukat *et al.*, "Development of -cyclodextrin/polyvinypyrrolidone-co-poly (2-acrylamide-2-methylpropane sulphonic acid) hybrid nanogels as nano-drug delivery carriers to enhance the solubility of rosuvastatin: An in vitro and in vivo evaluation," *PLOS ONE*, vol. 17, no. 1, p. e0263026, 2022.

[134] J. D. dos Santos Carvalho, R. S. Rabelo, and M. D. Hubinger, "Thermo-rheological properties of chitosan hydrogels with hydroxypropyl methylcellulose and methylcellulose," *International Journal of Biological Macromolecules*, vol. 209, pp. 367–375, 2022.

[135] X. Jiang *et al.*, "Preparation and characterization of photosensitive methacrylate-grafted sodium carboxymethyl cellulose as an injectable material to fabricate hydrogels for biomedical applications," *International Journal of Biological Macromolecules*, vol. 263, p. 130190, 2024.

[136] C. Pagano *et al.*, "Development of sodium carboxymethyl cellulose based polymeric microparticles for in situ hydrogel wound dressing formation," *International Journal of Pharmaceutics*, vol. 602, p. 120606, 2021.

[137] D. H. Hanna and G. R. Saad, "Encapsulation of ciprofloxacin within modified xanthan gum-chitosan based hydrogel for drug delivery," *Bioorganic Chemistry*, vol. 84, pp. 115–124, 2019.

[138] S. Naji-Tabasi, M. Shahidi-Noghabi, and A. M. Dovom, "Investigating the fabrication and functional properties of new composite hydrogels containing gellan/alginate/xanthan gum," *Journal of Sol-Gel Science and Technology*, vol. 105, no. 3, pp. 637–649, 2023.

[139] C. Cona, K. Bailey, and E. Barker, "Characterization methods to determine interpenetrating polymer network (ipn) in hydrogels," *Polymers*, vol. 16, no. 14, p. 2050, 2024.

[140] H. Shoukat *et al.*, "Development of -cyclodextrin/chitosan-co-poly (2-acrylamide-2-methylpropane sulphonic acid) cross-linked hybrid ipn-nanogels to enhance the solubility of rosuvastatin: An in vitro and in vivo attributes," *Journal of Drug Delivery Science and Technology*, vol. 75, p. 103696, 2022.

[141] M. Aslam *et al.*, "ph sensitive pluronic acid/agarose-hydrogels as controlled drug delivery carriers: design, characterization and toxicity evaluation," *Pharmaceutics*, vol. 14, no. 6, p. 1218, 2022.